A space-time BIE method for wave equation problems: the (two-dimensional) Neumann case

A space-time BIE method for wave equation problems. The (2D) Neumann case. *

S. Falletta†, G. Monegato‡, L. Scuderi§

Abstract

In this paper, initially we consider the (2D and 3D) interior and exterior problems for the scalar wave equation, with a Neumann boundary condition and in general with non trivial data. For these problems, we derive a space-time hypersingular boundary integral equation formulation. Then, in the 2D case, we propose a numerical approach for the computation of the extra "volume" integrals generated by the problem data. To solve the above integral equation in the 2D case, we propose to use a second order Lubich convolution quadrature for the discretization of the time integral, coupled with a (space) ϵ-collocation boundary element method. We also analyze the numerical evaluation of all the integrals required by this method.

Finally, to show the efficiency of the proposed numerical approach, and to detect its convergence rate, we solve some 2D test problems by applying the new method, as well as the corresponding Galerkin one. Several numerical examples are presented.

KEY WORDS: wave equation; Neumann problem; non homogeneous conditions; space-time boundary integral equations; numerical methods

1 Introduction

Let $\Omega^i \subset \mathbb{R}^d$, $d = 2, 3$, be an open bounded domain with a sufficiently smooth boundary Γ; define $\Omega^e = \mathbb{R}^d \setminus \bar{\Omega}^i$. Consider the following exterior problem given by the scalar wave equation with a Neumann boundary condition:

$$\begin{cases} \Delta u^e(\mathbf{x},t) - u^e_{tt}(\mathbf{x},t) &= f(\mathbf{x},t) \quad \text{in } \Omega^e \times (0,T) \\ \dfrac{\partial u^e}{\partial \mathbf{n}_e}(\mathbf{x},t) &= g(\mathbf{x},t) \quad \text{in } \Gamma \times (0,T) \\ u^e(\mathbf{x},0) &= u_0(\mathbf{x}) \quad \text{in } \Omega^e \\ u^e_t(\mathbf{x},0) &= v_0(\mathbf{x}) \quad \text{in } \Omega^e. \end{cases} \tag{1}$$

*This work was supported by the Ministero dell'Istruzione, dell'Università e della Ricerca of Italy, under the research program: Boundary element methods for time-dependent problems.

†Dipartimento di Scienze Matematiche, Politecnico di Torino, Italy. Email: silvia.falletta@polito.it

‡Dipartimento di Scienze Matematiche, Politecnico di Torino, Italy. Email: giovanni.monegato@polito.it

§Dipartimento di Scienze Matematiche, Politecnico di Torino, Italy. Email: letizia.scuderi@polito.it

where the data f, u_0, v_0 are smooth and, in general, but not necessarily, have compact supports. By extending smoothly the data f, u_0, v_0 into Ω^i, we associate with (1) the corresponding interior problem

$$\begin{cases} \Delta u^i(\mathbf{x},t) - u^i_{tt}(\mathbf{x},t) & = f(\mathbf{x},t) \quad \text{in } \Omega^i \times (0,T) \\ \dfrac{\partial u^i}{\partial \mathbf{n}_i}(\mathbf{x},t) & = -g(\mathbf{x},t) \quad \text{in } \Gamma \times (0,T) \\ u^i(\mathbf{x},0) & = u_0(\mathbf{x}) \quad \text{in } \Omega^i \\ u^i_t(\mathbf{x},0) & = v_0(\mathbf{x}) \quad \text{in } \Omega^i. \end{cases} \tag{2}$$

In (1) and (2), $\mathbf{n}_e$ and $\mathbf{n}_i$ denote the associated boundary outward unit normal vectors.

We recall that from a theoretical point of view, if the boundary Γ is sufficiently smooth, any smooth function defined in Ω^e can be smoothly extended on Ω^i, and vice versa, if this is required. From the practical point of view we assume that the data f, u_0, v_0 are defined in all of $\mathbb{R}^d$, or, for instance in the case of a data with compact support, that are trivially extended in $\mathbb{R}^d$.

Results on existence, uniqueness and regularity of the solutions of problems of this type can be found in [9], [22], [23].

For simplicity, in this paper we assume that the boundary Γ of the domain Ω (either Ω^e or Ω^i) and the data satisfy the regularity and compatibility properties which guarantee the existence and uniqueness of the solutions of both problems in $C^2(\bar{\Omega} \times [0,T])$. Nevertheless, when testing our numerical approach, we will apply it also to problems whose data do not satisfy all these assumptions.

In the following, we will initially consider both exterior and interior problems. Since in the applications we may have to deal not only with the homogeneous wave equation with trivial initial values, but also with non homogeneous problems, we will concentrate our attention mainly to these latter. Exterior non homogeneous problems arise, for example, when studying wave propagations outside of a scatterer or an obstacle Ω^i. About these problems see, for example, [36], [24], [16].

A time domain boundary element method, for an interior non homogeneous problem, has been very recently proposed for electromagnetic microwave simulations (see [19]). The problem data may have a global or a compact support. In the (3D) problem considered in [19], the wave equation known term f is even concentrated along a line.

In this paper, however, our main goal will be the numerical solution of exterior problems. Moreover, we will especially consider data having a global support; but we will also suggest a numerical approach for dealing with those that have a local support. This because it is the former case that produces the highest overhead computation with respect to the homogeneous case; furthermore, this is also the case where the volume integration can cause numerical difficulties when the time t becomes large.

To solve (interior and exterior) non homogeneous problems, in the next section we derive a space-time hypersingular boundary integral equation. Although space-time boundary integral formulations have been used for many years by engineers to solve homogeneous problems, the development of a satisfactory theory and of standard numerical tools for their solution is still far from being completed. For a survey on this topic see for example [13].

In the case of the 3D exterior problem for the homogeneous wave equation, with homogeneous initial conditions, in 1994 (see [26]) Lubich has proposed and examined

a new numerical approach to solve such problems when the boundary condition is the Dirichlet one. His method is based on a special (convolution) quadrature rule (see [25], [35]) he has constructed and examined, for the discretization of the time integral, and on a standard Galerkin BEM for the space integration. For his numerical scheme he has proved unconditional stability and convergence. In 2009 this theory has been applied by Chappell [11] also for the corresponding 3D Neumann problem. For further results see also [21]. These are the only known theoretical results. They all refer to 3D problems.

The use of a (space) collocation method is very appealing, because of its lower computational cost. Nevertheless, for this approach we are not aware of stability and convergence results in the case of the wave equation. We are not even aware of some significant numerical testing of these properties.

Lubich's approach has been also used to solve some homogeneous wave propagation problems in elastodynamics (see, for example, [37],[20],[40]). It has also stimulated the study of some fast algorithms for the implementation of the convolution quadrature/Galerkin method (see for example [10], [18]) for the 3D wave case, which take into account the lower block triangular Toeplitz structure of the final linear system and the behavior of its matrix elements.

However, except for a few papers written by engineers (see for example [28], [4], [3]), none of the above mentioned papers deals with the non homogeneous case of the wave equation. Moreover, in all these papers the numerical evaluation of the integrals generated by the proposed approaches is apparently ignored or simply taken for granted, although this is a fundamental issue for the success of the method. With respect to this evaluation, it is the 2D case that causes more difficulties.

Very recently (see [15]) we have considered the (2D and 3D) exterior problem for the non homogeneous wave equation, with a Dirichlet boundary condition and non homogeneous initial conditions. In particular, to solve this problem, we have first derived a space-time single-layer BIE formulation that takes into account the non trivial initial data. This gives rise to "volume" integrals, for whose evaluation an efficient numerical approach has been proposed. The above mentioned BIE has then been solved by coupling a second order Lubich discrete convolution quadrature with classical collocation and Galerkin BEMs.

From the testing we have performed in [15], and that we will present in Section 4, it appears that the CPU overhead due to the data volume integrals is often negligible or fairly low. This is even more true when the data have a local support. Moreover, for the potential evaluation, we have recently constructed and tested a new integration approach for the time integral (see [34]), having a very low computational cost. We believe that this BEM approach should provide, especially for the solution of the exterior problem, a viable alternative to the FEM method (possibly coupled with a non reflecting artificial boundary condition; see for example [16]). Although we are not aware of comparisons of this type, there are situations, like for example those mentioned in the introduction of [19], where a time domain BEM approach may provide attractive advantages. This should be also true when the solution of the original PDE problem is required only in a neighborhood of the boundary Γ, or in a small region away from Γ.

In the present paper we extend the numerical approach proposed in [15] to the case of problem (1). In particular, in Section 2 we derive a space-time hypersingular BIE to represent this problem and obtain, for the 2D case, simple representations for the

"volume" integrals generated by the initial data as well as by the equation known term. For the evaluation of these integrals we propose some efficient integration rules.

In Section 3 we examine and construct a second order Lubich convolution quadrature associated with the kernel of the above hypersingular BIE in the 2D case. This rule is then coupled with a (space) collocation method to solve homogeneous and non homogeneous problems. Since no (theoretical) stability and convergence results are known for the 2D collocation method, as well as for the 2D Galerkin method, to test these properties, in Section 4 we apply these methods to some simple 2D problems. This testing includes nodal collocation, ϵ-collocation and Galerkin methods (for the space discretization). Efficient numerical integration rules are proposed for the computation of all the integrals required by these methods. Some conclusions are finally drawn in Section 5.

2 A boundary integral equation formulation

In this paper we will consider smooth problems, of form (1) or (2), having C^2 solutions. In particular, we will solve problems defined on domains having a smooth boundary and sufficiently smooth compatible data, satisfying, for simplicity, at least the following conditions:

$$f \in C^1([0,T], C^3(\mathbb{R}^d)),\ g \in C^2([0,T], C(\Gamma)),\ v_0 \in C^3(\mathbb{R}^d),\ u_0 \in C^4(\mathbb{R}^d)$$

and, for all $\mathbf{x} \in \Gamma$,

$$g(\mathbf{x},0) = \frac{\partial u_0(\mathbf{x})}{\partial \mathbf{n}}, \qquad g_t(\mathbf{x},0) = \frac{\partial v_0(\mathbf{x})}{\partial \mathbf{n}}, \qquad g_{tt}(\mathbf{x},0) = \frac{\partial}{\partial \mathbf{n}}[\Delta u_0(\mathbf{x}) - f(\mathbf{x},0)]. \quad (3)$$

where $\mathbf{n} = \mathbf{n}_e$ in the case of the exterior problem, and $\mathbf{n} = \mathbf{n}_i$ when dealing with the interior one. These assumptions are required mainly to be able to apply existing theoretical results. However, in our numerical testing we will also consider data not satisfying all the above mentioned smoothness requirements. In any case, these are actually a little stronger than those really needed, but we have made them for notational simplicity. They will be used in the proof of Proposition 2.2 (see Sect. 2.2) to perform some simple Taylor expansions.

Let $G(\mathbf{x},t)$ denote the wave equation fundamental solution

$$G(\mathbf{x},t) = \frac{1}{2\pi}\frac{H(t-\|\mathbf{x}\|)}{\sqrt{t^2-\|\mathbf{x}\|^2}}, \qquad \mathbf{x} \in \mathbb{R}^2$$

$$G(\mathbf{x},t) = \frac{1}{4\pi\|\mathbf{x}\|}\delta(t-\|\mathbf{x}\|) = \frac{1}{4\pi\|\mathbf{x}\|}\frac{\partial}{\partial t}H(t-\|\mathbf{x}\|), \qquad \mathbf{x} \in \mathbb{R}^3,$$

$H(\cdot)$ and $\delta(\cdot)$ being the well known Heaviside and Dirac delta functions, respectively. Then, for the solution of problem (1) we have the following result.

Proposition 2.1 *Let $\Omega \subset \mathbb{R}^d$ be either Ω^i or Ω^e, and $[u(\mathbf{x},t)] = u^i(\mathbf{x},t) - u^e(\mathbf{x},t)$, $\mathbf{x} \in \Gamma$, denote the jump of the solution along the boundary. Let $\mathbf{n_y}(\mathbf{n_x})$ denote the outward (with respect to the chosen Ω domain) boundary unit normal vector evaluated*

at the point $\mathbf{y}(\mathbf{x}) \in \Gamma$. *Under the smoothness assumptions we have made above we have:*

$$\begin{aligned} u(\mathbf{x},t) &= \int_\Gamma \int_0^t \frac{\partial G}{\partial \mathbf{n_y}}(\mathbf{x}-\mathbf{y},t-\tau)[u(\mathbf{y},\tau)]\,d\tau\,d\Gamma_\mathbf{y} + \frac{\partial}{\partial t}\int_{\mathbb{R}^d} u_0(\mathbf{y})G(\mathbf{x}-\mathbf{y},t)d\mathbf{y} \quad (4)\\ &\quad + \int_{\mathbb{R}^d} v_0(\mathbf{y})G(\mathbf{x}-\mathbf{y},t)d\mathbf{y} - \int_{\mathbb{R}^d}\int_0^t f(\mathbf{y},\tau)G(\mathbf{x}-\mathbf{y},t-\tau)\,d\tau\,d\mathbf{y}, \quad \mathbf{x}\in\Omega, \end{aligned}$$

$$\begin{aligned} g(\mathbf{x},t) &= \frac{\partial}{\partial \mathbf{n_x}}\int_\Gamma\int_0^t \frac{\partial G}{\partial \mathbf{n_y}}(\mathbf{x}-\mathbf{y},t-\tau)[u(\mathbf{y},\tau)]\,d\tau\,d\Gamma_\mathbf{y} + \frac{\partial}{\partial \mathbf{n_x}}\frac{\partial}{\partial t}\int_{\mathbb{R}^d} u_0(\mathbf{y})G(\mathbf{x}-\mathbf{y},t)\,d\mathbf{y} \quad (5)\\ &\quad + \frac{\partial}{\partial \mathbf{n_x}}\int_{\mathbb{R}^d} v_0(\mathbf{y})G(\mathbf{x}-\mathbf{y},t)\,d\mathbf{y} - \frac{\partial}{\partial \mathbf{n_x}}\int_{\mathbb{R}^d}\int_0^t f(\mathbf{y},\tau)G(\mathbf{x}-\mathbf{y},t-\tau)\,d\tau\,d\mathbf{y}, \quad \mathbf{x}\in\Gamma. \end{aligned}$$

$$\begin{aligned} u(\mathbf{x},t) &= \int_\Gamma\int_0^t \frac{\partial G}{\partial \mathbf{n_y}}(\mathbf{x}-\mathbf{y},t-\tau)[u(\mathbf{y},\tau)]\,d\tau\,d\Gamma_\mathbf{y} + \frac{\partial}{\partial t}\int_{\mathbb{R}^d} u_0(\mathbf{y})G(\mathbf{x}-\mathbf{y},t)\,d\mathbf{y} \quad (6)\\ &+ \int_{\mathbb{R}^d} v_0(\mathbf{y})G(\mathbf{x}-\mathbf{y},t)\,d\mathbf{y} - \int_{\mathbb{R}^d}\int_0^t f(\mathbf{y},\tau)G(\mathbf{x}-\mathbf{y},t-\tau)\,d\tau\,d\mathbf{y} - \frac{1}{2}[u(\mathbf{x},t)] \quad \mathbf{x}\in\Gamma. \end{aligned}$$

In this latter expression we have $u(\mathbf{x},t) = u^e(\mathbf{x},t)$ *when* $\Omega = \Omega^e$, *and* $u(\mathbf{x},t) = u^i(\mathbf{x},t)$ *when* $\Omega = \Omega^i$.

Proof. Consider the integral equation formulations for the interior and exterior problems we have derived in [15]:

$$\begin{aligned} &\int_\Gamma\int_0^t G(\mathbf{x}-\mathbf{y},t-\tau)\partial_{\mathbf{n}_i}u^i(\mathbf{y},\tau)d\tau d\Gamma_\mathbf{y} - \int_\Gamma\int_0^t \partial_{\mathbf{n}_i}G(\mathbf{x}-\mathbf{y},t-\tau)u^i(\mathbf{y},\tau)\,d\tau\,d\Gamma_\mathbf{y} +\\ &\frac{\partial}{\partial t}\int_{\Omega^i} u_0(\mathbf{y})G(\mathbf{x}-\mathbf{y},t)d\mathbf{y} + \int_{\Omega^i} v_0(\mathbf{y})G(\mathbf{x}-\mathbf{y},t)\,d\mathbf{y} - \int_{\Omega^i}\int_0^t f(\mathbf{y},\tau)G(\mathbf{x}-\mathbf{y},t-\tau)\,d\tau\,d\mathbf{y}\\ &= \begin{cases} u^i(\mathbf{x},t) & \mathbf{x}\in\Omega^i\\ \frac{1}{2}u^i(\mathbf{x},t) & \mathbf{x}\in\Gamma\\ 0 & \mathbf{x}\in\Omega^e, \end{cases} \end{aligned} \quad (7)$$

and

$$\begin{aligned} &\int_\Gamma\int_0^t G(\mathbf{x}-\mathbf{y},t-\tau)\partial_{\mathbf{n}_e}u^e(\mathbf{y},\tau)d\tau d\Gamma_\mathbf{y} - \int_\Gamma\int_0^t \partial_{\mathbf{n}_e}G(\mathbf{x}-\mathbf{y},t-\tau)u^e(\mathbf{y},\tau)\,d\tau\,d\Gamma_\mathbf{y} +\\ &\frac{\partial}{\partial t}\int_{\Omega^e} u_0(\mathbf{y})G(\mathbf{x}-\mathbf{y},t)\,d\mathbf{y} + \int_{\Omega^e} v_0(\mathbf{y})G(\mathbf{x}-\mathbf{y},t)\,d\mathbf{y} - \int_{\Omega^e}\int_0^t f(\mathbf{y},\tau)G(\mathbf{x}-\mathbf{y},t-\tau)\,d\tau\,d\mathbf{y}\\ &= \begin{cases} 0 & \mathbf{x}\in\Omega^i\\ \frac{1}{2}u^e(\mathbf{x},t) & \mathbf{x}\in\Gamma\\ u^e(\mathbf{x},t) & \mathbf{x}\in\Omega^e, \end{cases} \end{aligned} \quad (8)$$

where u^i and u^e denote the solutions of the interior and exterior problems, respectively. Summing these two integral formulations, we obtain expression (4).

To obtain the double layer boundary integral equation formulation of (1), first we take the normal derivative $\partial \mathbf{n}_{\mathbf{x}}$ of both sides of (4). Then, letting $\mathbf{x} \in \Omega$ move to Γ, and computing properly this limit (see [12]), we finally have (5).

Once the unknown $[u(\mathbf{y}, \tau)]$ has been determined, one can compute $u(\mathbf{x}, t)$ at $\mathbf{x} \in \Omega$ by means of (4). If instead the goal is the value of $u^e(\mathbf{x}, t)$ at a point $\mathbf{x} \in \Gamma$, then from (8) and (7) one easily derives the representation (6).□

In Proposition (2.6) it will be shown that, under the assumptions we have made on the problem data, all the volume terms of the above representations are C^2 continuous with respect to their arguments $\mathbf{x}$ and t.

Remark 2.2 *To solve the exterior problem, for example, we could also use directly equation (8), which in this case is only weakly singular and of the second kind. However this equation requires, for any chosen* $\mathbf{x}$ *and* t*, also the computation of the corresponding (double) integral containing the known Neumann data. One has this overhead also when, later, the computation of the associated potential, i.e., the solution* $u^e(\mathbf{x}, t)$ *at points* $\mathbf{x} \in \Omega^e$*, must be performed.*

Moreover, as remarked in [15], because of the presence of the Heaviside function in the expression defining the kernel G*, in the case of data with "global" supports the formulations (7) and (8) require the computation of volume integrals defined on the intersection of the data supports with the disc (sphere) of radius* t *centered at* $\mathbf{x}$*; a task that is by no means trivial, unless* Ω *itself is a disc (sphere). In formulation (5), no matter what is the shape of the boundary* Γ*, the domain of integration of our volume integrals is a disc (sphere), which makes the integral calculation fairly simple.*

Because of the above two main reasons, to solve our problems we will use formulation (5). In this case we have to assume, as we did, that all the problem data are defined (after a smooth extension) in the whole space $\mathbb{R}^d$*.*

Notice that by considering different smooth extensions of the data f, u_0, v_0*, we obtain corresponding different known terms and unknown densities in the above formulations; nevertheless the associated potential* $u(\mathbf{x}, t)$ *will always be the same. This latter does not depend on the particular chosen extension of the data.*

Remark 2.3 *When a data has a local support, away from the boundary* Γ *for example, and decays smoothly to zero around the boundary support, for computational convenience we embed the support into a disc/sphere* $C(y_s, \rho_s)$*, with center at* y_s *and radius* ρ_s*, and consider this latter as practical support of the data. The (space) domain of integration for this data will then be: (i) empty, if* $t \leq \|x - y_s\| - \rho_s$*; (ii) coinciding with* $C(y_s, \rho_s)$*, when* $t \geq \|x - y_s\| + \rho_s$*; (iii) given by* $C(x, t) \cap C(y_s, \rho_s)$ *otherwise. Thus, in this case, the computational overhead required by these volume integrals will be significantly smaller than that required in the case of data with global supports. Moreover, the overhead would depend on the size of the data supports. For these reasons, in the following we will consider only the worst case, i.e., that of data having a global support. Nevertheless, the numerical evaluation of the volume integrals in the above local case will be briefly discussed at the end of the next section.*

For reasons of space, from now on we will examine only the 2D case. The 3D case will be treated in a forthcoming paper (see, however, the final comment in Section 5).

2.1 The volume terms

Concerning the volume terms due to the non homogeneous problem data, a key issue for the success of the overall numerical approach is their accurate and fast evaluation. To this end, in the following we analyze their representations given in (5), i.e.,

$$\begin{aligned} I_{u_0}(\mathbf{x},t) &= \frac{\partial}{\partial \mathbf{n_x}}\frac{\partial}{\partial t}\int_{\mathbb{R}^2} u_0(\mathbf{y})G(\mathbf{x}-\mathbf{y},t)\,d\mathbf{y} \\ I_{v_0}(\mathbf{x},t) &= \frac{\partial}{\partial \mathbf{n_x}}\int_{\mathbb{R}^2} v_0(\mathbf{y})G(\mathbf{x}-\mathbf{y},t)\,d\mathbf{y} \\ I_f(\mathbf{x},t) &= \frac{\partial}{\partial \mathbf{n_x}}\int_{\mathbb{R}^2}\int_0^t f(\mathbf{y},\tau)G(\mathbf{x}-\mathbf{y},t-\tau)\,d\tau\,d\mathbf{y} \end{aligned} \tag{9}$$

and, in the case of data with global supports, derive equivalent expressions which are more suitable for their evaluation. For these, in Section 3.2 we will propose some efficient quadrature rules.

For the cases mentioned in Remark 2.3, it is not difficult to derive corresponding representations. In these latter cases, we might have to deal with situations of nearly (strong) singularities, that have to be treated properly, if one wants to achieve the required accuracy with a low number of nodes. We remark however that, when the support is local, the space domain of integration is at most a disc/sphere of fixed radius ρ_s, not one of increasing radius t.

Lemma 2.4 *Let $r = \|\mathbf{x}-\mathbf{y}\| > 0$ and $t > 0$. Then the following representation holds:*

$$\frac{\partial G}{\partial \mathbf{n_x}}(\mathbf{x}-\mathbf{y},t) = -\frac{1}{2\pi}\left[\frac{\partial}{\partial t}\frac{H(t-r)}{\sqrt{t^2-r^2}} + \frac{(t-r)H(t-r)}{(t^2-r^2)^{3/2}}\right]\frac{\partial r}{\partial \mathbf{n_x}}. \tag{10}$$

Proof. Let $H_k(x)$ be, for example, the well known logistic function

$$H_k(x) = \frac{1}{1+e^{-2kx}}, \quad k \to \infty$$

which converges to the Heaviside function $H(x)$ both pointwise and in the weak sense. Then write

$$\frac{\partial}{\partial r}\left(\frac{H_k(t-r)}{\sqrt{t^2-r^2}}\right) = -\frac{H_k'(t-r)}{\sqrt{t^2-r^2}} + \frac{rH_k(t-r)}{(t^2-r^2)^{3/2}},$$

from which, recalling also the relationship

$$\frac{H_k'(t-r)}{\sqrt{t^2-r^2}} = \frac{\partial}{\partial t}\frac{H_k(t-r)}{\sqrt{t^2-r^2}} + \frac{tH_k(t-r)}{(t^2-r^2)^{3/2}},$$

we have

$$\frac{\partial}{\partial \mathbf{n_x}}\left(\frac{H_k(t-r)}{\sqrt{t^2-r^2}}\right) = -\left[\frac{\partial}{\partial t}\left(\frac{H_k(t-r)}{\sqrt{t^2-r^2}}\right) + \frac{(t-r)H_k(t-r)}{(t^2-r^2)^{3/2}}\right]\frac{\partial r}{\partial \mathbf{n_x}}.$$

Taking the weak limit of this latter, for $k \to \infty$, and applying the dominated convergence theorem, we finally obtain (10).□

By introducing the polar coordinates, centered at $\mathbf{y} = \mathbf{x}$:

$$\mathbf{y} = \mathbf{y}_r = \mathbf{x} + r\mathbf{e}_\theta, \qquad \mathbf{e}_\theta = (\cos\theta, \sin\theta)^T,$$

recalling the definition of finite part integral, here and in the following denoted by the symbol $\fint$, and the relation (see [31], Sect.3)

$$\frac{d}{dt} \fint_0^t \frac{r f(\mathbf{y}_r)}{(t^2 - r^2)^{m/2}} dr = -mt \fint_0^t \frac{r f(\mathbf{y}_r)}{(t^2 - r^2)^{m/2+1}} dr, \quad 0 < r < t$$

where $m \geq 1$ is an integer, and the left hand side integral is a Riemann one when $m = 1$, we obtain new representations for the volume integrals defined in (9), more suitable for their evaluation.

Proposition 2.5 *Let* $\mathbf{n}_\mathbf{x} = (n_{\mathbf{x},1}, n_{\mathbf{x},2})^T$ *and* $t > 0$. *Then the following representations holds:*

$$I_{v_0}(\mathbf{x}, t) = -\frac{1}{2\pi} \int_0^{2\pi} (n_{\mathbf{x},1}\cos\theta + n_{\mathbf{x},2}\sin\theta) \fint_0^1 \frac{\xi^2}{(1-\xi)^{3/2}} \frac{v_0(\mathbf{x} + t\xi\mathbf{e}_\theta)}{(1+\xi)^{3/2}} d\xi d\theta, \tag{11}$$

$$I_{u_0}(\mathbf{x}, t) = \frac{3}{2\pi t} \int_0^{2\pi} (n_{\mathbf{x},1}\cos\theta + n_{\mathbf{x},2}\sin\theta) \fint_0^1 \frac{\xi^2}{(1-\xi)^{5/2}} \frac{u_0(\mathbf{x} + t\xi\mathbf{e}_\theta)}{(1+\xi)^{5/2}} d\xi d\theta. \tag{12}$$

$$I_f(\mathbf{x}, t) = -\frac{t}{2\pi} \int_0^{2\pi} (n_{\mathbf{x},1}\cos\theta + n_{\mathbf{x},2}\sin\theta) \fint_0^1 \frac{\xi^2}{(1-\xi)^{3/2}} \frac{F(\mathbf{x}, t; \theta, \xi)}{(1+\xi)^{3/2}} d\xi d\theta. \tag{13}$$

In the latter we have set

$$F(\mathbf{x}, t; \theta, \xi) = \int_0^1 f(\mathbf{x} + t\xi(1-\tau)\mathbf{e}_\theta, t\tau) d\tau \tag{14}$$

Proof. By using relationship (10), for I_{v_0} in (9) we have:

$$\begin{aligned}
&I_{v_0}(\mathbf{x}, t) \\
&= -\frac{1}{2\pi} \frac{\partial}{\partial t} \int_{\mathbb{R}^2} v_0(\mathbf{x} + r\mathbf{e}_\theta) \frac{H(t-r)}{\sqrt{t^2 - r^2}} \frac{\partial r}{\partial \mathbf{n}_\mathbf{x}} d\mathbf{y} - \frac{1}{2\pi} \int_{\mathbb{R}^2} v_0(\mathbf{x} + r\mathbf{e}_\theta) \frac{(t-r)H(t-r)}{(t^2 - r^2)^{3/2}} \frac{\partial r}{\partial \mathbf{n}_\mathbf{x}} d\mathbf{y} \\
&= -\frac{1}{2\pi} \int_0^{2\pi} (n_{\mathbf{x},1}\cos\theta + n_{\mathbf{x},2}\sin\theta) \left(t \fint_0^t \frac{r v_0(\mathbf{x} + r\mathbf{e}_\theta)}{(t^2 - r^2)^{3/2}} dr - \int_0^t \frac{r v_0(\mathbf{x} + r\mathbf{e}_\theta)}{\sqrt{t-r}(t+r)^{3/2}} dr \right) d\theta \\
&= -\frac{1}{2\pi} \int_0^{2\pi} (n_{\mathbf{x},1}\cos\theta + n_{\mathbf{x},2}\sin\theta) \times \\
&\left(\fint_0^1 \frac{1}{(1-\xi)^{3/2}} \frac{\xi v_0(\mathbf{x} + t\xi\mathbf{e}_\theta)}{(1+\xi)^{3/2}} d\xi - \int_0^1 \frac{\xi v_0(\mathbf{x} + t\xi\mathbf{e}_\theta)}{\sqrt{1-\xi}(1+\xi)^{3/2}} d\xi \right) d\theta
\end{aligned}$$

i.e. (11), where we have set $r = t\xi$. We recall that in the above finite part integrals the change of variable is allowed, even if the hypersingularity is at an endpoint, because the order of the singularity is not an integer (see [30], p.13).

Analogously we get

$$I_{u_0}(\mathbf{x},t) = -\frac{1}{2\pi}\frac{\partial^2}{\partial t^2}\int_{\mathbb{R}^2} u_0(\mathbf{x}+r\mathbf{e}_\theta)\frac{H(t-r)}{\sqrt{t^2-r^2}}\frac{\partial r}{\partial \mathbf{n}_\mathbf{x}}d\mathbf{y}$$
$$-\frac{1}{2\pi}\frac{\partial}{\partial t}\int_{\mathbb{R}^2} u_0(\mathbf{x}+r\mathbf{e}_\theta)\frac{H(t-r)}{\sqrt{t-r}(t+r)^{3/2}}\frac{\partial r}{\partial \mathbf{n}_\mathbf{x}}d\mathbf{y} =: I_1 + I_2$$

hence derive the expressions

$$I_1 = -\frac{1}{2\pi t}\int_0^{2\pi}(n_{\mathbf{x},1}\cos\theta + n_{\mathbf{x},2}\sin\theta)\left(\Xint=_0^1 \frac{\xi u_0(\mathbf{x}+t\xi\mathbf{e}_\theta)}{(1-\xi^2)^{3/2}}d\xi - 3\Xint=_0^1 \frac{\xi u_0(\mathbf{x}+t\xi\mathbf{e}_\theta)}{(1-\xi^2)^{5/2}}d\xi\right)d\theta$$

$$I_2 = -\frac{1}{4\pi t}\int_0^{2\pi}(n_{\mathbf{x},1}\cos\theta + n_{\mathbf{x},2}\sin\theta)\left(\Xint=_0^1 \frac{\xi u_0(\mathbf{x}+t\xi\mathbf{e}_\theta)}{(1-\xi^2)^{3/2}}d\xi + 3\Xint=_0^1 \frac{\xi u_0(\mathbf{x}+t\xi\mathbf{e}_\theta)}{\sqrt{1-\xi}(1+\xi)^{5/2}}d\xi\right)d\theta.$$

From these it follows that

$$I_{u_0}(\mathbf{x},t) = -\frac{3}{4\pi t}\int_0^{2\pi}(n_{\mathbf{x},1}\cos\theta + n_{\mathbf{x},2}\sin\theta)\times$$
$$\left(\Xint=_0^1 \frac{\xi u_0(\mathbf{x}+t\xi\mathbf{e}_\theta)}{(1-\xi^2)^{3/2}}d\xi + \Xint=_0^1 \frac{\xi(\xi^2-2\xi-1)u_0(\mathbf{x}+t\xi\mathbf{e}_\theta)}{(1-\xi^2)^{5/2}}d\xi\right)d\theta$$

i.e., (12).

The integral $I_f(\mathbf{x},t)$ is very similar to $I_{v_0}(\mathbf{x},t)$, except for an extra (inner) integration over $(0,t)$.□

The numerical evaluation of the above integrals will be discussed in Section 3.2. When the data have local supports (as described in Remark 2.3), the corresponding volume integrals are different from zero only when $t > \|x-y_s\| - \rho_s$. In this case, they are represented by expressions very similar to those reported above, where now the θ interval of integration is of the type $(\theta_1,\theta_2),\ \theta_1 > 0, \theta_2 < 2\pi$, while that of the r variable is of the form $(r_0(\theta),t)$ if $t \le \|x-y_s\| + \rho_s$, and $(r_0(\theta),r_1(\theta))$ otherwise. The values of r_0, r_1 are determined, for each of the above values of θ, by intersecting the line, defined by the point $\mathbf{x}$ and the angle θ, with the circle $C(y_s,\rho_s)$. Notice that in the case $t < \|x-y_s\| + \rho_s$, to avoid the splitting of the θ interval into three parts, for simplicity we have enlarged a little bit the domain of integration, by adding to it a small region where the integrand is null.

2.2 The hypersingular BIE representation

Recalling the definition of finite part integral (see [31]), and the smoothness properties of our problems, the BIE (5) can be rewritten in the following hypersingular form:

$$\Xint=_\Gamma\int_0^t \frac{\partial^2 G}{\partial \mathbf{n}_\mathbf{x}\partial \mathbf{n}_\mathbf{y}}(\mathbf{x}-\mathbf{y},t-\tau)\varphi(\mathbf{y},\tau)\,d\tau\,d\Gamma_\mathbf{y} = \bar{g}(\mathbf{x},t), \quad \mathbf{x}\in\Gamma,\ t\in[0,T],$$
$$\bar{g}(\mathbf{x},t) = g(\mathbf{x},t) - I_{u_0}(\mathbf{x},t) - I_{v_0}(\mathbf{x},t) + I_f(\mathbf{x},t) \tag{15}$$

where the density function $\varphi(\mathbf{y},\tau) = [u(\mathbf{y},\tau)]$ is sought on Γ, and I_{v_0}, I_{u_0} and I_f have been defined in Section 2.1.

Next we derive the (expected) consequences that the compatibility conditions (3) have on the right hand side of equation (15). As we shall shortly recall, in the 3D case, the (unconditional) stability and convergence properties derived in [11] for the Lubich/Galerkin BEM require the function $\bar{g}(\cdot,t)$, together with a certain number of its time derivatives, to vanish on Γ for $t=0$.

Proposition 2.6 *Under the assumptions made above on the problem data we have* $I_{u_0}, I_{v_0}, I_f \in C^2([0,T], C(\mathbb{R}^2))$*; moreover, for all* $\mathbf{x}\in\Gamma$ *the following conditions are satisfied:*

$$\begin{aligned}
&I_{u_0}(\mathbf{x},0) = \frac{\partial u_0(\mathbf{x})}{\partial \mathbf{n_x}}, && \frac{\partial I_{u_0}(\mathbf{x},0)}{\partial t} = 0, && \frac{\partial^2 I_{u_0}(\mathbf{x},0)}{\partial t^2} = \frac{\partial}{\partial \mathbf{n_x}}\Delta u_0(\mathbf{x}),\\
&I_{v_0}(\mathbf{x},0) = 0, && \frac{\partial I_{v_0}(\mathbf{x},0)}{\partial t} = \frac{\partial v_0(\mathbf{x})}{\partial \mathbf{n_x}}, && \frac{\partial^2 I_{v_0}(\mathbf{x},0)}{\partial t^2} = 0,\\
&I_f(\mathbf{x},0) = 0, && \frac{\partial I_f(\mathbf{x},0)}{\partial t} = 0, && \frac{\partial^2 I_f(\mathbf{x},0)}{\partial t^2} = \frac{\partial f(\mathbf{x},0)}{\partial \mathbf{n_x}}.
\end{aligned} \tag{16}$$

Hence in (15) we have $\bar{g}\in C^2([0,T], C(\Gamma))$ *with*

$$\bar{g}(\mathbf{x},0) = \frac{\partial \bar{g}(\mathbf{x},0)}{\partial t} = \frac{\partial^2 \bar{g}(\mathbf{x},0)}{\partial t^2} = 0. \tag{17}$$

Proof. Recalling the identity:

$$\frac{d}{dt}\,\text{⨍}_0^1 \frac{\xi^m}{(1-\xi^2)^{n/2}} h(\mathbf{x}+\alpha t\xi)d\xi = \text{⨍}_0^1 \frac{\xi^m}{(1-\xi^2)^{n/2}} \frac{d}{dt} h(\mathbf{x}+\alpha t\xi)d\xi, \quad m\geq 0,\ n\geq 3$$

that can be easily derived from the definition of finite part integral (see [31]), and performing Taylor expansions on $f(\mathbf{y}_r) = f(\mathbf{x}+re_\theta)$, some lengthy and cumbersome calculation leads to the results stated above.□

Remark 2.7 *Assume that the data of our problem are sufficiently smooth, to perform the required Taylor expansions, i.e.,*

$$f\in C^{\ell-1}([0,T], C^{\ell+1}(\mathbb{R}^2)),\ g\in C^{\ell}([0,T], C(\Gamma)),\ v_0\in C^{\ell+1}(\mathbb{R}^2),\ u_0\in C^{\ell+2}(\mathbb{R}^2)$$

for some integer $\ell\geq 2$*, and that they satisfy corresponding compatibility conditions of order up to* $m\leq \ell$*, to guarantee that problems (1) and (2) have* C^ℓ *solutions. Then, by means of the same machinery used to prove Proposition 2.2, one can easily show that* $\bar{g}\in C^\ell([0,T], C(\mathbb{R}^2))$*, with* $\bar{g}(\mathbf{x},0) = \frac{d}{dt}\bar{g}(\mathbf{x},0) = \cdots = \frac{d^m}{dt^m}\bar{g}(\mathbf{x},0) = 0$.

Having shown that the right hand side of (15) satisfies (at least) the homogeneous compatibility conditions (17), and taking into account the above remark, we are now ready to solve (15) using a second order Lubich's discrete convolution rule.

We recall, that for the solution of an hypersingular space-time BIE of type (15), in the 3D case Chappell in [11], following Lubich's approach, has associated the Lubich second order BDF convolution quadrature, having constant stepsize Δ_t, with a classical Galerkin method for the space discretization. In particular, to define this latter, he has discretized the boundary Γ by a quasiuniform partition with element diameter Δ_x and

considered a corresponding piecewise polynomial approximant of local degree $k \geq 1$. Having denoted by $\varphi_n(y)$ the approximant determined by the above Lubich/Galerkin method at the time instant $t_n = n\Delta_t$, by assuming that the problem data satisfy certain smoothness and compatibility conditions, such that for the corresponding known term in (15) we have $\bar{g} \in H^{\mu}(0,T;H^{-1/2}(\Gamma))$, with $\mu > 9/2$ and $\frac{d^i}{dt^i}\bar{g}(\cdot,t) = 0, i \leq 4$, he has then been able to derive the following (unconditional) convergence estimate:

$$\|\varphi_n - \varphi(\cdot, n\Delta_t)\|_{H^{1/2}(\Gamma)} \leq C_T \left(\Delta_t^2 + \Delta_x^{k+1/2}\right), \tag{18}$$

where the (positive) constant C_T depends on T, but not on n, Δ_t, Δ_x. We recall however that, taking advantage of part (ii) of Theorem 3.1 in [26], and writing

$$\bar{g}(\cdot,t) = \frac{\bar{g}^{(4)}(\cdot,0)}{4!}t^4 + \bar{g}_1(\cdot,t)$$

in the above conditions on $\bar{g}$, the requirement $i \leq 3$ is sufficient (although not necessary, as the numerical testing we have performed seems to confirm). Therefore in Remark 2.7 it is sufficient to take $\ell = 5, m = 3$; in this case we define the data *compatible*.

As for the Dirichlet problem, no results have been derived for the Galerkin method in the 2D case and for corresponding collocation methods. In the Dirichlet case, the numerical testing performed in [15] seems to suggest that results analogous to (18) should hold also in the 2D Galerkin case and for a collocation method. Therefore, in the next section we will construct a Lubich/collocation method of local degree 1, that, associated with the second order Lubich BDF rule, will then be used in Section 4 to solve some 2D test problems. The same problems will be solved also using the corresponding Galerkin method. The stability and convergence properties of the method will then be tested in this latter section.

3 Discretization using convolution quadrature in time and collocation in space

3.1 The homogeneous case

As recalled in Section 2, to solve a problem of type (1), or (2), having compatible data, with $u_0 = 0, v_0 = 0, f = 0$, we have at our disposal the following two BIE representations, for $\mathbf{x} \in \Gamma$:

$$\begin{aligned} \frac{1}{2}u^e(\mathbf{x},t) + \int_\Gamma \int_0^t \frac{\partial G}{\partial \mathbf{n_y}}(\mathbf{x}-\mathbf{y}, t-\tau)u^e(\mathbf{y},\tau)\,d\tau\,d\Gamma_\mathbf{y} \\ = \int_\Gamma \int_0^t G(\mathbf{x}-\mathbf{y}, t-\tau)g(\mathbf{y},\tau)\,d\tau\,d\Gamma_\mathbf{y} \end{aligned} \tag{19}$$

for the exterior problem and

$$\begin{aligned} -\frac{1}{2}u^i(\mathbf{x},t) + \int_\Gamma \int_0^t \frac{\partial G}{\partial \mathbf{n_y}}(\mathbf{x}-\mathbf{y}, t-\tau)u^i(\mathbf{y},\tau)\,d\tau\,d\Gamma_\mathbf{y} \\ = \int_\Gamma \int_0^t G(\mathbf{x}-\mathbf{y}, t-\tau)g(\mathbf{y},\tau)\,d\tau\,d\Gamma_\mathbf{y} \end{aligned} \tag{20}$$

for the interior problem. Both integral equations are of the second kind.

Alternatively, as shown in Section 2, we can describe both problems by associating with them the following hypersingular (boundary) integral equation of the first kind:

$$\neq\!\!\!\!\int_\Gamma \int_0^t \frac{\partial^2 G}{\partial \mathbf{n_x} \partial \mathbf{n_y}}(\mathbf{x}-\mathbf{y}, t-\tau)\phi(\mathbf{y},\tau)\, d\tau\, d\Gamma_{\mathbf{y}} = g(\mathbf{x},t),\ \mathbf{x}\in\Gamma \tag{21}$$

where $\phi(\mathbf{y},\tau) := [u(\mathbf{x},\tau)]$. For the properties of this equation, in the 3D case, see [11].

In Section 4, of all the formulas we have proposed to compute the required integrals, and of the convolution quadrature-collocation method, we will apply both approaches to solve two homogeneous problems (see Examples 1 and 2). In particular, we will compare the accuracies and the rates of convergence of the approximations we obtain for the corresponding solutions.

In the following, after having set $t = t_n = n\Delta_t, \Delta_t = T/N$, $T > 0$ being fixed, we will use a second order (BDF) Lubich discrete convolution quadrature (see [26]) to discretize the inner integral on $(0, t_n)$. This rule has the form

$$\int_0^{t_n} k(t_n-\tau)\varphi(\tau)d\tau \approx \sum_{j=0}^{n} \omega_{n-j}(\Delta_t)\varphi(j\Delta_t),\ n=0,\dots,N. \tag{22}$$

The kernel $k(t)$ is assumed to have a Laplace transform $K(s)$ analytic in a region of the form $\Re(s) > \sigma_0$, where it has also to satisfy a bound of the type: $|K(s)| \le C|s|^{-\mu}$, μ real. We recall that if $\mu > 0$ then the kernel k is certainly locally integrable and we have

$$\int_0^t k(t-\tau)\varphi(\tau)d\tau = \frac{1}{2\pi\imath}\int_{\sigma+\imath\mathbb{R}} K(s)x(t;s)ds, \tag{23}$$

for any $\sigma > \sigma_0$, where

$$x(t;s) = \int_0^t e^{s(t-\tau)}\varphi(\tau)d\tau.$$

When $\mu \le 0$, however, as we shall see shortly, the above identity (23) still holds, as long as the function φ is sufficiently smooth and the integral over $\sigma+\imath\mathbb{R}$ is interpreted in the finite part sense. In this case, as pointed out in [27], having defined m to be the smallest integer such that $m+\mu > 0$, under the assumption $\varphi \in C^m[0,T]$ we ought to set

$$\int_0^t k(t-\tau)\varphi(\tau)d\tau = \frac{d^m}{dt^m}\int_0^t k_1(t-\tau)\varphi(\tau)d\tau \tag{24}$$

where

$$k_1(t) = \frac{1}{2\pi\imath}\int_{\sigma+\imath\mathbb{R}} \frac{K(s)}{s^m}e^{st}ds.$$

For the coefficients of rule (22), the following representation:

$$\omega_n(\Delta_t) = \frac{1}{2\pi\imath}\int_{|z|=\rho} K\left(\frac{\gamma(z)}{\Delta_t}\right) z^{-(n+1)}\, dz \tag{25}$$

where ρ is such that the circle $|z| \le \rho$ lies in the domain of analyticity of $K(\gamma(z)/\Delta_t)$, has been derived in [25] (see also [35]).

Remark 3.1 *In the 2D case, the Laplace transforms $K = \widehat{k}, K = K(r;s)$, of the kernels $k = G, \frac{\partial G}{\partial \mathbf{n_y}}, \frac{\partial^2 G}{\partial \mathbf{n_x}\partial \mathbf{n_y}}$, which appear in the above three BIE formulations, can be computed by using some well known properties of the modified Bessel functions (see formulas 8.486(11,16,17) in [17]). In particular, setting $r = \|x\| > 0$, for $G(\mathbf{x}, t)$ we have*

$$\begin{aligned} \widehat{G}(r,s) &= \frac{1}{2\pi} K_0(rs), \\ \widehat{\frac{\partial G}{\partial \mathbf{n_y}}}(r,s) &= -\frac{1}{2\pi} s K_1(rs) \frac{\partial r}{\partial \mathbf{n_y}}, \end{aligned} \tag{26}$$

where $K_0(z)$ and $K_1(z)$ are the second kind modified Bessel function of order 0 and 1, respectively, and

$$\widehat{\frac{\partial^2 G}{\partial \mathbf{n_x}\partial \mathbf{n_y}}}(r,s) = \frac{s^2}{2\pi} \left[\left(K_0(rs) + \frac{1}{rs} K_1(rs) \right) \frac{\partial r}{\partial \mathbf{n_x}} \frac{\partial r}{\partial \mathbf{n_y}} - \frac{1}{s} K_1(rs) \frac{\partial^2 r}{\partial \mathbf{n_x}\partial \mathbf{n_y}} \right]. \tag{27}$$

For any given $r > 0$, these three Laplace transforms are analytic in $\Re(s) > \sigma_0 > 0$, with σ_0 arbitrarily small. Moreover, recalling the behavior of the Bessel functions K_0, K_1 (see [1]), in this domain we have:

$$|K(s)| \le C \begin{cases} |s|^{-1/2}, & k = G & \left(\mu = \frac{1}{2}\right), \\ |s|^{1/2}, & k = \frac{\partial G}{\partial \mathbf{n_y}} & \left(\mu = -\frac{1}{2}\right), \\ |s|^{3/2}, & k = \frac{\partial^2 G}{\partial \mathbf{n_x}\partial \mathbf{n_y}} & \left(\mu = -\frac{3}{2}\right), \end{cases}$$

Therefore, because of these behaviors, and the degrees of smoothness of Γ and $\phi(\mathbf{y}, \tau)$, one is allowed to exchange the order of integration in the left hand sides of (19), (20), (21) only if, after the exchange, the inner integral over $(0, t)$ is interpreted (in the finite part sense) as defined above in (24).

Lemma 3.2 *(see [39] p. 229). For any given non negative integer ℓ, and any given real $r > 0$, we have :*

$$\frac{1}{2\pi\imath} \int_{\sigma+\imath\mathbb{R}} \frac{K_\nu(rs)}{s^\ell} ds = 0, \quad \nu = 0, 1,$$

where K_ν denotes the modified Bessel function of the second kind of order ν.

In the following Proposition we give an explicit expression of the finite part integral defined in (24), when the kernel k is either $\frac{\partial G}{\partial \mathbf{n_y}}$, which corresponds to the case $m = 1$ in (24), or $\frac{\partial^2 G}{\partial \mathbf{n_x}\partial \mathbf{n_y}}$ $(m = 2)$.

Proposition 3.3 *Let $\varphi \in C^2[0, T]$, with $\varphi(0) = 0$. Let k be either $\frac{\partial G}{\partial \mathbf{n_y}}$ $(m = 1)$ or $\frac{\partial^2 G}{\partial \mathbf{n_x}\partial \mathbf{n_y}}$ $(m = 2)$ and $K(s)$ be its Laplace transform. Then the following representation holds:*

$$\int_0^t k(t-\tau)\varphi(\tau) d\tau = \frac{d^m}{dt^m} \int_0^t k_1(t-\tau)\varphi(\tau) d\tau = \frac{1}{2\pi\imath} \int_{\sigma+\imath\mathbb{R}} K(s) x(t;s) ds$$

where in the case $m = 2$ the last integral is defined in the finite part sense, i.e.,

$$\frac{1}{2\pi\imath} \oint\!\!\!\!\!\!= \int_{\sigma+\imath\mathbb{R}} K(s)x(t;s)ds = \frac{1}{2\pi\imath} \int_{\sigma+\imath\mathbb{R}} K(s) \left[x(t;s) + \frac{\varphi(t)}{s} \right] ds$$

Proof. First we write (24) as follows:

$$I := \frac{1}{2\pi\imath} \int_{\sigma+\imath\mathbb{R}} \quad \frac{K(s)}{s^m} \frac{d^m}{dt^m} x(t;s)ds, \quad m = 1, 2,$$

and notice that, having assumed $\varphi \in C^2[0,T]$, with $\varphi(0) = 0$, we have

$$x(t;s) + \frac{\varphi(t)}{s} = \frac{x_1(t;s)}{s^2}$$

with

$$|x_1(t;s)| \leq C \quad \text{for } s \in \sigma + \imath\mathbb{R},$$

uniformly with respect to $t \in [0,T]$.

Thus, taking advantage of the relationship

$$\frac{d}{dt} x(t;s) = sx(t;s) + \varphi(t)$$

and recalling Lemma 3.2, we obtain the expressions:

$$I = \frac{1}{2\pi\imath} \begin{cases} \displaystyle\int_{\sigma+\imath\mathbb{R}} K(s)x(t;s)ds, & m = 1, \\ \displaystyle\int_{\sigma+\imath\mathbb{R}} K(s) \left[x(t;s) + \frac{\varphi(t)}{s} \right] ds, & m = 2, \end{cases}$$

where both integrals are defined in the usual sense. □

Remark 3.4 *In the case of the kernel (27) ($m = 2$), only the component containing the term $s^2 K_0(rs)$ can give rise to a finite part integral. This happens however only in the representation of the coefficient $\omega_0(\Delta_t)$ (see [35], p.415), whose value turns out to be given by the expression:*

$$\omega_0(\Delta_t) = \widehat{\frac{\partial^2 G}{\partial \mathbf{n_x} \partial \mathbf{n_y}}}(r, \alpha_0/\Delta_t) = \tag{28}$$
$$\frac{1}{2\pi} \frac{\alpha_0}{\Delta_t} \left\{ \left[\frac{\alpha_0}{\Delta_t} K_0 \left(\frac{r\alpha_0}{\Delta_t} \right) + \frac{1}{r} K_1 \left(\frac{r\alpha_0}{\Delta_t} \right) \right] \frac{\partial r}{\partial \mathbf{n_x}} \frac{\partial r}{\partial \mathbf{n_y}} - K_1 \left(\frac{r\alpha_0}{\Delta_t} \right) \frac{\partial^2 r}{\partial \mathbf{n_x} \partial \mathbf{n_y}} \right\}$$

where $\alpha_0 = \frac{3}{2}$ is the constant term of the characteristic polynomial $\gamma(z) = \frac{3}{2} - 2z + \frac{1}{2}z^2$ associated with the chosen second order Backward Differentiation Formula (BDF) for ODE (see [26]). For the other components, as well as for all those defining the coefficients $\omega_{n-j}, j = 0, \ldots, n-1$, the corresponding Bromwich integrals are defined in the usual sense and the corresponding Lubich's rule coefficients can be determined by using Lubich's approach.

After noticing that

$$\frac{\partial r}{\partial \mathbf{n_x}} \sim r, \quad \frac{\partial r}{\partial \mathbf{n_y}} \sim r, \quad \frac{\partial^2 r}{\partial \mathbf{n_x} \partial \mathbf{n_y}} \sim r^{-1}, \qquad r \to 0,$$

and recalling that (see (40) below)

$$K_1(rs) \sim r^{-1},\ s > 0 \text{ fixed},$$

from the representation (28) it follows that the coefficient ω_0 have a second order hypersingularity at the origin, i.e., for $\Delta_t > 0$ fixed,

$$\omega_0(\Delta_t) = \omega_0(\Delta_t; r) \sim r^{-2},\ r \to 0.$$

Further, recalling the behaviors of the K Bessel functions and of their derivatives near the origin (see [1]), it can be shown that also the following coefficients $\omega_n(\Delta_t), n \geq 1$, have the same hypersingularity.

After these preliminary remarks, we are now entitled to construct (BDF) Lubich rules associated with these new 2D kernels, since they are all well defined.

We recall that in the case of our kernels, and in particular of the one which gives rise to the above finite part integral, representation (25) holds also for $\omega_0(\Delta_t)$. Indeed, Lubich's derivation of this representation automatically defines its finite part explicitly given in Remark 3.4. Of course we can use the formula given in Remark 3.4 to determine directly the value of ω_0 with machine precision, since in principle when we apply the trapezoidal rule, as suggested in [26], to the representation (25), some numerical cancelation could appear; however, in practice this does not seem to be the case.

We consider first formulation (19). To solve it numerically, for the time discretization we split the interval $[0, T]$ into N steps of equal length $\Delta_t = T/N$ and collocate the equation at the discrete time levels $t_n = n\Delta_t$, $n = 0, \ldots, N$:

$$\begin{aligned} \frac{1}{2}u^e(\mathbf{x}, t_n) + \int_\Gamma \int_0^{t_n} \frac{\partial G}{\partial \mathbf{n}_\mathbf{y}}(\mathbf{x} - \mathbf{y}, t_n - \tau) u^e(\mathbf{y}, \tau)\, d\Gamma_\mathbf{y}\, d\tau \\ = \int_\Gamma \int_0^{t_n} G(\mathbf{x} - \mathbf{y}, t_n - \tau) g(\mathbf{y}, \tau)\, d\Gamma_\mathbf{y}\, d\tau. \end{aligned} \tag{29}$$

The time integrals are then discretized by means of the Lubich convolution quadrature associated with the BDF method of order $p = 2$. We obtain:

$$\sum_{j=0}^{n} \int_\Gamma \omega_{n-j}(\Delta_t; ||\mathbf{x} - \mathbf{y}||) u^e(\mathbf{y}, t_j)\, d\Gamma_\mathbf{y}, \quad n = 0, \ldots, N \tag{30}$$

where coefficients ω_n are given by (see (25)):

$$\omega_n(\Delta_t; ||\mathbf{x} - \mathbf{y}||) = \frac{1}{2\pi i} \int_{|z|=\rho} K\left(||\mathbf{x} - \mathbf{y}||, \frac{\gamma(z)}{\Delta_t}\right) z^{-(n+1)}\, dz,$$

K being the Laplace transform of $\partial G/\partial \mathbf{n}_\mathbf{y}$ for the integral to the left hand side of (29), and of G for the integral to the right hand side.

For the space discretization, first we introduce the parametrization of the curve Γ, $\mathbf{x} = \boldsymbol{\psi}(x) = (\psi_1(x), \psi_2(x))$ and $\mathbf{y} = \boldsymbol{\psi}(y) = (\psi_1(y), \psi_2(y))$ with $x, y \in [a, b]$, and then we approximate the unknown function $u^e_{\Delta_t}$ by

$$u^e_{\Delta_t}(\boldsymbol{\psi}(x), t_j) \approx \sum_{k=1}^{M+1} u^e_{j\,k} N_k(x), \quad x \in [a, b] \tag{31}$$

where $N_k(x)$ are the shape functions, in our case, for simplicity, of linear type, defined on a uniform partition $\{x_h\}_{h=1}^{M+1}$ of the parametrization interval $[a,b] = [x_1, x_{M+1}]$, with mesh size Δ_x. Taking into account that the curve Γ is closed, we have $\boldsymbol{\psi}(x_1) = \boldsymbol{\psi}(x_{M+1})$ and $u^e_{j\,1} = u^e_{j\,M+1}$. Therefore, having set $x_0 = x_1 - \Delta_x$, hence extended by periodicity the function $\boldsymbol{\psi}(x)$, so that $\boldsymbol{\psi}(x_0) = \boldsymbol{\psi}(x_M)$, we replace the sum in (31) by

$$\sum_{k=1}^{M} u^e_{j\,k} N_k(x), \quad x \in [x_0, x_{M+1}],$$

and the interval of integration by (x_0, x_{M+1}).

Finally, by collocating the fully discretized equation at the points $\xi_h = x_h$, $h = 1, \ldots, M$, we obtain a Toeplitz block lower triangular linear system of the form:

$$\sum_{j=0}^{n-1} \mathbf{A}_{n-j} \mathbf{u}^e_j + \left(\frac{1}{2}\mathbf{I} + \mathbf{A}_0\right) \mathbf{u}^e_n = \mathbf{g}_n, \quad n = 0, \ldots, N \tag{32}$$

in the unknown vectors $\mathbf{u}^e_j = (u^e_{j\,1}, \ldots, u^e_{j\,M})$, $j = 0, \ldots, n$, where the sum is empty when $n = 0$, and $\mathbf{I}$ denotes the identity matrix of order M. From the computational point of view this takes the form

$$\left(\frac{1}{2}\mathbf{I} + \mathbf{A}_0\right) \mathbf{u}^e_n = \mathbf{g}_n - \sum_{j=0}^{n-1} \mathbf{A}_{n-j} \mathbf{u}^e_j, \quad n = 0, \ldots, N \tag{33}$$

with

$$(\mathbf{A}_{n-j})_{hi} = \int_{x_0}^{x_{M+1}} \omega_{n-j}(\Delta_t; \|\boldsymbol{\psi}(x_h) - \boldsymbol{\psi}(y)\|) N_i(y) |\boldsymbol{\psi}'(y)| dy.$$

In particular the matrix $\mathbf{A}_0$, the only one that needs to be inverted, is defined by the coefficient ω_0, for which an explicit representation has been given in Remark 3.4.

As suggested in [26], the above convolution coefficients ω_n can be efficiently computed by means of the trapezoidal rule

$$\omega_n(\Delta_t; ||\mathbf{x} - \mathbf{y}||) \approx \frac{\rho^{-n}}{L} \sum_{l=0}^{L-1} K\left(||\mathbf{x} - \mathbf{y}||, \frac{\gamma(\rho e^{\imath \frac{l2\pi}{L}})}{\Delta_t}\right) e^{-\imath n \frac{l2\pi}{L}} \tag{34}$$

where the interval $(0, 2\pi)$ has been partitioned into L subintervals of equal length. All the ω_n can be computed simultaneously by the FFT with $O(N \log N)$ flops.

Assuming that K is computed with a relative accuracy bounded by ε, in the case $|K(s)| \leq C|s|^{-\mu}$, $\mu \geq 0$, Lubich in [26] has proposed the choice

$$L = 2N, \quad \rho = \varepsilon^{\frac{1}{2N}} \tag{35}$$

to obtain an error of size $O(\sqrt{\varepsilon})$ in the approximation of ω_n.

Since in the case of our hypersingular equation we have $\mu < 0$, one should examine the corresponding error bound as in [25], Sect. 7. This has been done, for example, in [11], where for the 3D case Chappell takes $L = N + 1$ and $\rho \approx \epsilon^{1/N}$. Other choices of ρ, suggested in [11] and [10], did not produce any improvements in our numerical testing. Thus, also because of the different behaviors of the three components in (27),

we have chosen the values (35). These have actually produced, at least in the examples we have considered, an accuracy very similar, and in some cases even superior, to that given by other choices. We remark however that the existence of a possible "optimal" choice of the values of the parameters L and ρ is still an open question.

Remark 3.5 *As we shall shortly see, for $s \neq 0$ the functions $K(r,\cdot)$, are weakly singular at $r = 0$. Therefore, to use the above approximation (34), in the final form of our collocation method we need to exchange the trapezoidal summation with the integral over Γ. Then, the FFT algorithm will be used to compute, simultaneously, all the terms of the summation over j.*

Thus, the collocation linear system takes the following form:

$$\begin{aligned}
&\frac{1}{2}\sum_{k=1}^{M} u^e_{n\,k} N_k(x_h) + \\
&\sum_{j=0}^{n} \rho^{j-n} \sum_{k=1}^{M} \frac{u^e_{j\,k}}{L} \sum_{l=0}^{L-1} \left[\int_{x_0}^{x_{M+1}} K^{(1)}\left(r_h, \frac{\gamma(\rho e^{\imath \frac{l2\pi}{L}})}{\Delta_t} \right) N_k(y) |\boldsymbol{\psi}'(y)|\, dy \right] e^{-\imath(n-j)\frac{l2\pi}{L}} \\
&= \sum_{j=0}^{n} \frac{\rho^{j-n}}{L} \sum_{l=0}^{L-1} \left[\int_{x_1}^{x_{M+1}} K^{(2)}\left(r_h, \frac{\gamma(\rho e^{\imath \frac{l2\pi}{L}})}{\Delta_t} \right) g(\boldsymbol{\psi}(y), t_j) |\boldsymbol{\psi}'(y)|\, dy \right] e^{-\imath(n-j)\frac{l2\pi}{L}}, \\
&h = 1, \ldots, M, \quad n = 0, \ldots, N
\end{aligned} \tag{36}$$

where $r_h = ||\boldsymbol{\psi}(x_h) - \boldsymbol{\psi}(y)||$. For $s \neq 0$, both kernels are analytic functions of $r > 0$. At $r = 0$

$$K^{(1)}(r,s) = -\frac{1}{2\pi} s K_1(rs) \frac{\partial r}{\partial \mathbf{n_y}} \tag{37}$$

has a mild singularity of the type $r^2 \ln r$, which however cannot be factored out, while (see [1])

$$K^{(2)}(r,s) = \frac{1}{2\pi} K_0(rs) \sim \ln r. \tag{38}$$

Also in this case the term $\ln r$ does not appear as a factor.

Since a key point for the success of the method is the accurate evaluation of all the integrals appearing in (36), possibly using a low number of quadrature points, in the following we will propose an efficient numerical approach for the computation of these integrals. This aspect of the problem does not seem to have been considered in the papers that have been published till now. Therefore, in the following we will treat carefully this aspect of the problem.

To this end, we preliminarily remark that all the weak singularities of our kernels cannot be factored out, and therefore they cannot be taken as weight functions of the corresponding integrals we have to compute. This means that the use of associated (weighted) Gaussian rules is not an efficient approach. To compute these integrals we will use the very simple and efficient polynomial smoothing technique proposed in [32], [33].

The numerical integration difficulties spring from the asymptotic behaviors of the K Bessel functions near the origin, given by the following representations (see [1], p.375):

$$\begin{aligned} K_0(z) &= -\left(\ln\frac{z}{2}+\gamma\right) I_0(z) + \sum_{k=1}^{\infty} a_k \frac{\left(\frac{z^2}{4}\right)^k}{(k!)^2} \\ I_0(z) &= \sum_{k=0}^{\infty} \frac{\left(\frac{z^2}{4}\right)^k}{(k!)^2}, \quad a_1 = 1,\ a_{k+1} = a_k + \frac{1}{k+1} \end{aligned} \tag{39}$$

$$\begin{aligned} K_1(z) &= \frac{1}{z} + \left(\ln\frac{z}{2}\right) I_1(z) - \frac{z}{4}\sum_{k=0}^{\infty} [\psi(k+1)+\psi(k+2)] \frac{\left(\frac{z^2}{4}\right)^k}{k!(k+1)!} \\ I_1(z) &= \frac{z}{2}\sum_{k=0}^{\infty} \frac{\left(\frac{z^2}{4}\right)^k}{k!(k+1)!} \end{aligned} \tag{40}$$

where $\psi(1) = -\gamma$, $\gamma = 0.5772156649...$ being the well known Euler's constant, and $\psi(k+1) = \psi(k) + 1/k$ (see [1]).

For the computation of the first integral in (36), i.e. that containing the kernel $K^{(1)}$, we rewrite it in the form:

$$\left(\int_{x_{k-1}}^{x_k} + \int_{x_k}^{x_{k+1}}\right) K^{(1)}\left(||\boldsymbol{\psi}(x_h) - \boldsymbol{\psi}(y)||, \frac{\gamma(\rho e^{\imath\frac{l2\pi}{L}})}{\Delta_t}\right) |\boldsymbol{\psi}'(y)| N_k(y)\, dy. \tag{41}$$

Since, when $h_k - 1, k, k+1$, $K^{(1)}$ has only a very mild singularity of the type $r^2 \log r$ at the collocation abscissa x_h, while it is smooth for all other values of h, we apply a n-point Gauss-Legendre rule, in general with n small, to each mesh element belonging to the support of N_k. To evaluate the integral

$$\int_a^b K^{(2)}\left(||\boldsymbol{\psi}(x_h) - \boldsymbol{\psi}(y)||, \frac{\gamma(\rho e^{\imath\frac{l2\pi}{L}})}{\Delta_t}\right) |\boldsymbol{\psi}'(y)| g(\boldsymbol{\psi}(y), t_j)\, dy, \tag{42}$$

because of the presence of a $\log r$ singularity, in the two subintervals of (a,b) having x_h as endpoint, i.e. in (a, x_h) and (x_h, b), we introduce preliminarily the *q-smoothing change of variable* $y = x_h \pm t^q$, $q = 3$, with the sign minus (plus) when x_h is the upper (lower) integration endpoint, and then we apply to each one of them a n-point Gauss-Legendre quadrature rule, in general with n not small as in the previous case.

The latter numerical procedure allows to use a number of quadrature nodes significantly smaller than that required by the direct application of the Gauss-Legendre rule, to obtain the same accuracy. Moreover, it does not require the decomposition of the kernels, in order to extract explicitly the weakly singular factor $\log r$. Because of its simplicity and effectiveness, we have preferred this approach to the use of a Gaussian rule with a $\log r$ weight. This idea has been successfully used to compute integrals of weakly singular functions, and also to solve, by standard polynomial methods, one-dimensional weakly singular integral equations (see, for example, [32], [33]).

Moreover, as Figure 1 below shows, to obtain an acceptable BIE numerical solution, the right hand side of the final linear system must be computed with a sufficiently

high accuracy, otherwise unwanted oscillations, caused by the errors generated by the known term integration, soon appear. To this end, the introduction of the q-smoothing transformation plays a crucial role, since it allows to reach the required accuracy using a significantly smaller number of quadrature nodes.

The case of representation (20) is very similar, therefore we omit it. Instead we consider the alternative case given by the hypersingular equation (21).

By coupling the Lubich convolution quadrature with a space collocation method, based on linear shape functions defined on a uniform partition of the parametrization interval, we obtain a linear system of the form:

$$\sum_{j=0}^{n} \bar{\mathbf{A}}_{n-j} \boldsymbol{\phi}_j = \bar{\mathbf{g}}_n, \quad n = 0, \ldots, N \tag{43}$$

whose structure is, as we can see, very similar to that of (32), with

$$(\bar{\mathbf{A}}_{n-j})_{hi} = \int_{x_0}^{x_{M+1}} = \omega_{n-j}(\Delta_t; \|\boldsymbol{\psi}(x_h) - \boldsymbol{\psi}(y)\| N_i(y) |\boldsymbol{\psi}'(y)| dy, \qquad (\bar{\mathbf{g}}_n)_h = g(\mathbf{x}_h, t_n). \tag{44}$$

Figure 1: u^e defined by (19); $M = 32$, $N = 16$, 64-point Gauss-Legendre rule with $q = 1$ (left) and $q = 3$ (right).

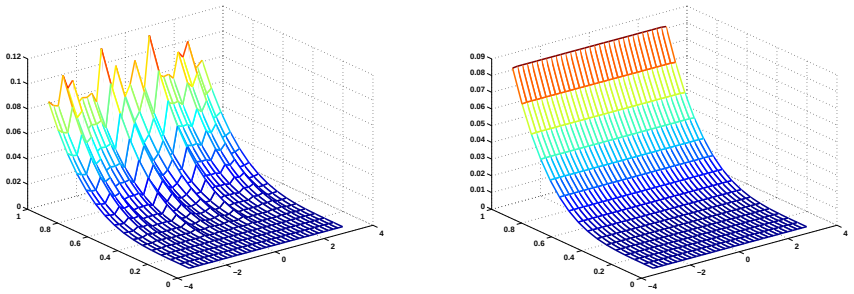

Remark 3.6 *We recall that in equation (21) the function ϕ is assumed to be smooth, and the hypersingular integral is defined as a two-sided finite part integral (see [29]). In this case it coincides with the sum of two one-sided finite part integrals, each one having the hypersingularity at one of the domain of integration endpoints. Moreover, equation (21) defines an identity between two continuous functions. When we replace the unknown ϕ by a continuous piecewise linear approximant, the above statement still holds, as long as x does not coincide with one of the mesh points x_k. If $x = x_k$, then the hypersingular integral can be defined only as the sum of two one-sided finite part integrals. In this case the two-sided finite part integral does not exist (see [29]). Nevertheless, we will investigate also this situation.*

The coefficients $\omega_{n-j}(\Delta_t; r)$ depend on $n-j$, not on n and j separately. This means that once we have constructed system (43), if we advance further in the time direction

by the same stepsize Δ_t, we only need to construct the new matrix $\bar{\mathbf{A}}_N$ and solve a new system of the form

$$\bar{\mathbf{A}}_0 \boldsymbol{\phi}_{N+1} = \bar{\mathbf{g}}_{N+1} - \sum_{j=1}^{N} \bar{\mathbf{A}}_{N+1-j} \boldsymbol{\phi}_j. \tag{45}$$

If however one wants to change Δ_t, then all the computation has to be restarted from $t = 0$. This is the main drawback of Lubich's convolution rule.

After replacing, as in the previous case, the ω_{n-j} coefficients by their approximation (34), system (43) takes the final form:

$$\begin{aligned} &\sum_{j=0}^{n} \rho^{j-n} \sum_{k=1}^{M} \frac{\phi_{j\,k}}{L} \sum_{l=0}^{L-1} \left[\int_{x_0}^{x_{M+1}} \overline{K} \left(||\boldsymbol{\psi}(\xi_h) - \boldsymbol{\psi}(y)||, \frac{\gamma(\rho e^{\imath \frac{l2\pi}{L}})}{\Delta_t} \right) N_k(y) |\boldsymbol{\psi}'(y)|\, dy \right] e^{-\imath(n-j)\frac{l2\pi}{L}} \\ &= g(\boldsymbol{\psi}(\xi_h), t_n), \qquad h = 1, \ldots, M, \quad n = 0, \ldots, N, \end{aligned} \tag{46}$$

where (see(27))

$$\begin{aligned} \overline{K}(r,s) = \frac{s^2}{2\pi} K_0(sr) \frac{\partial r}{\partial \mathbf{n_x}} \frac{\partial r}{\partial \mathbf{n_y}} + \frac{s}{2\pi r} K_1(sr) \frac{\partial r}{\partial \mathbf{n_x}} \frac{\partial r}{\partial \mathbf{n_y}} - \frac{s}{2\pi} K_1(sr) \frac{\partial^2 r}{\partial \mathbf{n_x} \partial \mathbf{n_y}} \\ =: K_D^{(1)}(r,s) + K_D^{(2)}(r,s) + K_D^{(3)}(r,s) \end{aligned} \tag{47}$$

and the $\{\xi_h\}$ are the chosen collocation points.

As collocation points we consider two choices: $\xi_h = x_h$ and $\xi_h = x_h + \epsilon \Delta_x$, with $0 < \epsilon < 1$. The associated methods will be called *nodal collocation* and ϵ-*collocation*, respectively. We will use the term *collocation method* to refer to both of them.

For $s \neq 0$, the kernels $K_D^{(1)}$ and $K_D^{(2)}$ in (47), as a function of r, are analytic for $r > 0$ and bounded at $r = 0$. Instead, the kernel $K_D^{(3)}$ has a r^{-2} hypersingularity at $r = 0$. Therefore, a remark similar to Remark 3.5 applies; however, since in this case the last kernel is hypersingular, the associated integral must be defined in the finite part sense in the boundary element containing the hypersingularity (ϵ-collocation) or having this latter at one of its endpoints (nodal collocation).

As before, for the computation of the integrals with the kernels $K_D^{(1)}$ and $K_D^{(2)}$ we have applied the n-point Gauss Legendre quadrature rule, with a low number of quadrature nodes, as it will be specified in the numerical examples we will present in Section 4.

The computation of the (hypersingular) integral defined by the kernel $K_D^{(3)}$ is far more delicate, and may cause a severe loss of accuracy if not treated properly. Thus, we propose to proceed as follows.

After noting that

$$\begin{aligned} &\frac{\partial^2 r}{\partial \mathbf{n_x} \partial \mathbf{n_y}}\Big|_{\mathbf{x}=\boldsymbol{\xi}_h} = -\frac{1}{r_h} f(r_h) \\ &f(r_h) := \frac{1}{r_h^2} \left\{ [\psi_2(\xi_h) - \psi_2(y)]^2 n_{\boldsymbol{\xi}_h,1} n_{\mathbf{y},1} + [\psi_1(\xi_h) - \psi_1(y)]^2 n_{\boldsymbol{\xi}_h,2} n_{\mathbf{y},2} \right. \\ &\left. -[\psi_1(\xi_h) - \psi_1(y)][\psi_2(\xi_h) - \psi_2(y)][n_{\boldsymbol{\xi}_h,1} n_{\mathbf{y},2} + n_{\boldsymbol{\xi}_h,2} n_{\mathbf{y},1}] \right\}, \end{aligned} \tag{48}$$

where we have set $\boldsymbol{\xi}_h = \boldsymbol{\psi}(\xi_h)$ and $r_h = \|\boldsymbol{\xi}_h - \mathbf{y}\|$, we obtain

$$I^{(3)} := \int_{x_{k-1}}^{x_{k+1}} K_D^{(3)}(r_h, s) N_k(y) |\boldsymbol{\psi}'(y)| dy = \frac{1}{2\pi} \int_{x_{k-1}}^{x_{k+1}} \frac{s r_h K_1(s r_h) f(r_h)}{r_h^2} N_k(y) |\boldsymbol{\psi}'(y)| dy. \tag{49}$$

When $\xi_h \in [x_{k-1}, x_{k+1}]$, this integral is defined in the finite part sense. In this case we write

$$\begin{aligned} I^{(3)} &= \frac{1}{2\pi} \, \text{⨍}_{x_{k-1}}^{x_{k+1}} s^2 f(r_h) N_k(y) \left[\frac{s r_h K_1(s r_h) - 1}{(s r_h)^2} + \frac{1}{(s r_h)^2} \right] |\boldsymbol{\psi}'(y)| dy \\ &= \frac{1}{2\pi} \int_{x_{k-1}}^{x_{k+1}} s^2 f(r_h) N_k(y) \frac{s r_h K_1(s r_h) - 1}{(s r_h)^2} |\boldsymbol{\psi}'(y)| dy + \frac{1}{2\pi} \, \text{⨍}_{x_{k-1}}^{x_{k+1}} \frac{f(r_h) N_k(y)}{r_h^2} |\boldsymbol{\psi}'(y)| dy \\ &=: I_1^{(3)} + I_2^{(3)} \end{aligned}$$

Since the term $zK_1(z)-1$ gives rise to a severe numerical cancellation when z is close to zero, which in turn has then a destroying effect on the overall integral computation, to overcome this drawback, when z is small we take advantage of expansion (40) and define

$$\frac{zK_1(z) - 1}{z^2} \approx \frac{1}{2} \sum_{k=0}^{N_0} \left[\ln \frac{z}{2} - \psi(k+1) - \frac{1}{2(k+1)} \right] \frac{\left(\frac{z^2}{4}\right)^k}{k!(k+1)!} \tag{50}$$

with N_0 chosen according to the approximation accuracy one wants to achieve. We remark that for z small the above series converges very fast, so that the required N_0 is actually very small. For example, using the 16-digit double precision arithmetic, for $|z| \leq 0.1$, choosing $N_0 = 4$ we obtain full machine accuracy. This happens also when $|z| \leq 10^{-4}$, if we choose $N_0 = 1$. On the contrary, if we use directly the expression $(zK_1(z) - 1)/z^2$, for $|z| > 0.1$ the numerical cancelation does not occur; for $10^{-3} \leq |z| \leq 10^{-1}$ we may have a loss of up to four significant digits, while for $|z| \leq 10^{-8}$ we loose all the significant figures.

To compute $I_1^{(3)}$ we use the numerical approach proposed for the computation of the previous integrals; that is, we introduce preliminarily the q-smoothing change of variable with $q = 5$ and then we apply an n-point Gauss-Legendre quadrature rule. To show the efficiency of this approach, in Table 1 we have reported the relative errors obtained in the computation of the following integral

$$\int_0^1 \frac{xK_1(x) - 1}{x^2} \, dx \tag{51}$$

by means of the q-smoothing transformation t^q and the n-point Gauss Legendre quadrature rule. Notice that in the first column of Table 1, where no transformation has been considered ($q = 1$), the accuracy increases very slowly; in the second column, where $q = 5$, the accuracy is better than the previous one, but it deteriorates because of the above mentioned numerical cancellation as the number of quadrature nodes increases. Finally, in the third column, where $q = 5$ and we have used the above expansion with $N_0 = 1$ when $x = t^q \leq 10^{-3}$, we obtain 14 significant digits by using only 32 Gaussian nodes. We notice however that the accuracy of the integral approximations given by the values $q = 5$ and $n = 8$ is already much higher than that required by the chosen BIE approximate solution.

Table 1: relative errors for (51)

n	$q=1$	$q=5$	$q=5,\ N_0=1$
4	$1.86E-02$	$1.17E-04$	$1.17E-04$
8	$5.19E-03$	$5.84E-07$	$3.19E-08$
16	$1.37E-03$	$5.98E-08$	$4.27E-11$
32	$3.54E-04$	$8.33E-08$	$7.40E-14$
64	$8.99E-05$	$8.73E-08$	$--$
128	$2.26E-05$	$6.34E-04$	$--$
256	$5.68E-06$	$8.10E-05$	$--$
512	$1.42E-06$	$3.63E-07$	$--$

The symbol $--$ means that the full relative accuracy has been reached. As reference value we have taken that given by $q=5$, $N_0=10$ and 512 Gaussian points.

Of course, one could apply an alternative approach based on the use of a Gauss-Legendre rule and of a Gaussian rule with a $\log x$ weight function; however, because of its simplicity and efficiency, we have preferred the one described above.

When, for example, $h=k$, to compute $I_2^{(3)}$ we write

$$I_2^{(3)} = \frac{1}{2\pi}\left[\fint_{x_{k-1}}^{x_k} + \fint_{x_k}^{x_{k+1}} \right] \Phi(y;\xi_k)\frac{F(y;\xi_k)}{(y-\xi_k)^2}dy \tag{52}$$

where we have set

$$\Phi(y;\xi_k) = \frac{(y-\xi_k)^2}{r_k^2}, \qquad F(y;\xi_k) = f(r_k)N_k(y)|\psi'(y)|,$$

and the first integral is defined in finite part sense only in the nodal collocation case. The hypersingular integrals are then computed by using the Radau type Gaussian rule defined in [30], with n Gaussian points. In the ϵ-collocation case, the (Riemann) integral over (x_{k-1},x_k) is evaluated using an n-point Gauss-Legendre formula. The case $h=k-1$ is very similar.

Note that in these two cases, to evaluate $\Phi(y;\xi_h)$ accurately, i.e. to avoid the numerical cancelation phenomenon, which inevitably appears when y is very close to the collocation point ξ_h, in general one has to compute it by using the Taylor expansion of the (smooth) functions $\psi_i(y), i=1,2$, around $y=\xi_h$. When $\xi_h \notin [x_{k-1},x_{k+1}]$, both integrals in (52) are Riemann and we compute them by using a n-point Gauss-Legendre rule.

Remark 3.7 *We have considered*

$$K^{(2)}(r,s) = \frac{1}{2\pi}K_0(sr)$$

and the following main components of the other Laplace transforms:

$$K^{(1)}(r,s) \doteq -\frac{1}{2\pi}srK_1(sr), \qquad K_D^{(1)}(r,s) \doteq \frac{1}{2\pi}(sr)^2K_0(sr),$$

$$K_D^{(2)}(r,s) \doteq \frac{1}{2\pi}srK_1(sr), \qquad K_D^{(3)}(r,s) \doteq -\frac{1}{2\pi}\frac{s}{r}K_1(sr).$$

For the ω-coefficients associated with these we have the property:

$$\omega_n(\Delta_t) = \omega_n(\Delta_t, r) = c_{\Delta_t}\omega_n(1, d), \quad d = \frac{r}{\Delta_t}$$

with $c_{\Delta_t} = 1$ in all cases except the last one, where $c_{\Delta_t} = \Delta_t^{-2}$. Thus, as we already did for the Dirichlet case, here we report a few graphs (see Figures 2-3) representing some behaviors of the original coefficients $\omega_n(1, d)$, i.e., those associated with the (full) Laplace transforms $K^{(1)}, K^{(2)}, K_D^{(1)}, K_D^{(2)}, K_D^{(3)}$.

Notice that the behavior of these coefficients is very similar to that of the corresponding ones defined by the Dirichlet problem (see [35]).

Figure 2: $\omega_n(1, 20),\ n = 0 : 100.$

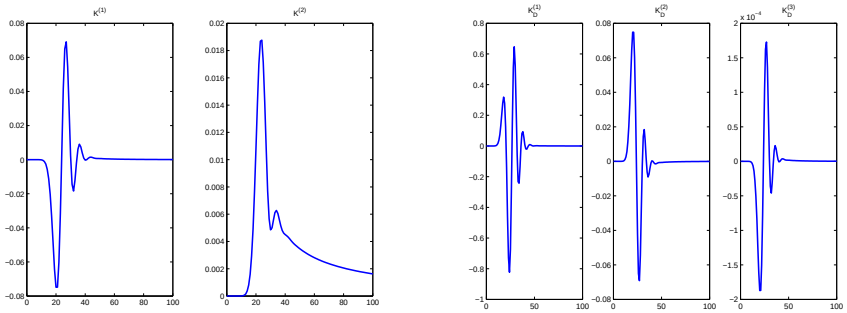

Figure 3: $\omega_{100}(1, d),\ d = 0.001 : 200.$

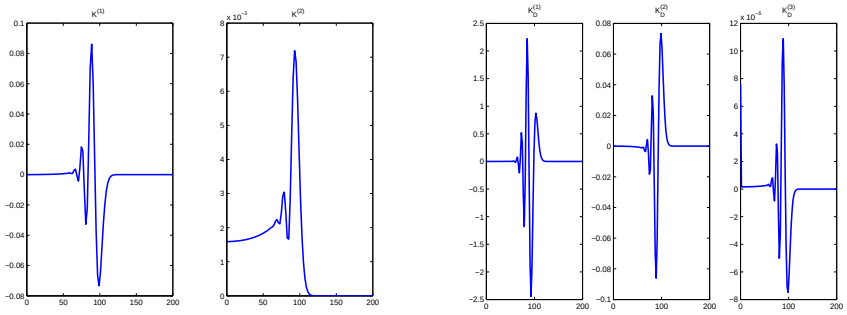

In this section, for the homogeneous case, we have presented two alternative BIE representations for the original PDE problem. However, as we shall point out in Section 4, Example 1, formulation (21) turns out to be, from all points of view, the most convenient one.

3.2 The non homogeneous case

In the non homogeneous case, it is even more true that the most convenient BIE representation is by far the hypersingular one. For its time discretization we split the

interval $[0,T]$ into N steps of equal length $\Delta_t = T/N$ and collocate the equation at the discrete time levels $t_n = n\Delta_t$, $n = 0,\ldots,N$, and at the chosen (collocation) points ξ_h.

The time integrals are then discretized by means of the Lubich convolution quadrature associated with the BDF method of order $p = 2$, while the unknown density function is, at each given instant $\tau = t_n$, approximated by a (continuous) piecewise linear function. After this, one proceeds exactly as in the homogeneous case, except that now extra volume integrals must be computed at each time level t_n and for each collocation point $\psi(\xi_h)$. Thus here we propose an efficient numerical approach for the evaluation of the integrals defined in Subsection 2.1.

For the inner finite-part integral we have at our disposal two alternative quadrature formulas: rules (2.10) and (2.16) of reference [30]. The first one is of Gauss-Radau type, while the second is only of interpolatory type. For some properties of them see [30]. In particular we propose to use the Gauss-Radau type rule for the evaluation of the integrals of form

$$⨍_0^1 \frac{\xi^2}{\sqrt{1-\xi}}\,\frac{\Phi(\xi)}{1-\xi}d\xi,$$

that is,

$$⨍_0^1 \frac{\xi^2}{\sqrt{1-\xi}}\,\frac{\Phi(\xi)}{1-\xi}d\xi \approx c_0\Phi(1) + \frac{1}{2\sqrt{2}}\sum_{i=1}^{n} w_i^{(1)}\Phi\left(\frac{1-\zeta_i}{2}\right)$$

with

$$c_0 = -\frac{16}{3} - \frac{1}{2\sqrt{2}}\sum_{i=1}^{n}\frac{\lambda_i}{1+\zeta_i} < 0$$

$$w_i^{(1)} = \frac{\lambda_i}{1+\zeta_i}$$

where $\{\lambda_i\},\{\zeta_i\}$ are the weights and nodes of the classical n-point Gauss-Jacobi quadrature rule defined in $(-1,1)$ and associated with the weight function $(1+\xi)^2(1-\xi)^{-1/2}$, respectively.

For the integral of form

$$⨍_0^1 \frac{\xi^2}{\sqrt{1-\xi}}\,\frac{\Psi(\xi)}{(1-\xi)^2}d\xi$$

one can use both quadrature rules. However, the Gaussian one requires also the evaluation of $\Psi'(1)$. Thus, to avoid this evaluation, we propose to use the second rule, which in our case takes the following form:

$$⨍_0^1 \frac{\xi^2}{\sqrt{1-\xi}}\,\frac{\Psi(\xi)}{(1-\xi)^2}d\xi \approx \sum_{i=1}^{n} w_i^{(2)}\Psi\left(\frac{1-\zeta_i}{2}\right) \tag{53}$$

where

$$w_i^{(2)} = \frac{\lambda_i}{\sqrt{2}(1+\zeta_i)^2} + \frac{\gamma_n}{(1+\zeta_i)P_{n-1}^{(3,1/2)}(\zeta_i)}\left\{2c_0\left[n+\frac{5}{2}-\frac{1}{n(1+\zeta_i)}\right]-\frac{c_1}{n}\right\} \tag{54}$$

$$\gamma_n = \frac{(-1)^n 4\Gamma(n+\frac{1}{2})}{\sqrt{\pi}(2n+5)(n-1)!}$$

$$c_1 = \frac{16}{3} - \frac{1}{\sqrt{2}}\sum_{i=1}^{n}\frac{\lambda_i}{(1+\zeta_i)^2} < 0$$

$c_0, \{\lambda_i\}, \{\zeta_i\}$ being defined as in the previous case, and $P_{n-1}^{(3,1/2)}(\zeta)$ is the $(n-1)$-degree Jacobi polynomial $P_{n-1}^{(\alpha,\beta)}(\zeta)$ with $\alpha = 3$ and $\beta = 1/2$ (see [1], Ch. 22). The values $\{P_{n-1}^{(3,1/2)}(\zeta_i)\}$ can be computed efficiently using the three-term recurrence relationship (see [1], Sect. 22.7) which defines these polynomials.

Notice that, taking the same number of nodes n in the above two quadrature rules, one can obtain a unique global integration rule for evaluation of the sum $I_{u_0} + I_{v_0}$, which is given by an expression of the following form:

$$\frac{1}{2\pi}\int_0^{2\pi}(n_{\mathbf{x},1}\cos\theta + n_{\mathbf{x},2}\sin\theta)\left[\frac{3}{2t}\fint_0^1\frac{\xi^2}{\sqrt{1-\xi}}\,\frac{\Psi(\xi,\theta)}{(1-\xi)^2}d\xi - \fint_0^1\frac{\xi^2}{\sqrt{1-\xi}}\,\frac{\Phi(\xi,\theta)}{1-\xi}d\xi\right]d\theta.$$

The inner integration over the time interval $(0,t)$ in I_f can be performed by using the Gauss-Legendre formula.

In all cases, the integrals defined on the interval $(0,2\pi)$ are evaluated using the classical trapezoidal rule. In the examples we will present in the next section, we have applied this formula with $2n$ abscissas, where n denotes the number of nodes used by the other quadrature rules described above. With this choice we had results slightly more accurate than those given by the n-point rule. We cannot exclude that a number of nodes lower than $2n$ would have given the same accuracy, but we have made this choice for simplicity. When a data has a local support, since the θ interval of integration in this case is of the type (θ_1,θ_2), with $0 < \theta_1 < \theta_2 < 2\pi$, the trapezoidal rule is replaced by the Gauss-Legendre one.

Remark 3.8 *Recalling Remark 2.7, we observe that when we take a time step Δ_t too small, the evaluation of the right hand side of equation (15) at the initial time instants, in particular at $t = t_1$, can generate numerical cancelation, whose effects will inevitably propagate at the subsequent instants and deteriorate the solution approximation, unless the volume integrals are evaluated with the needed accuracy. In the numerical examples we will present in the next section this phenomenon has shown up for values of Δ_t much smaller that those considered there.*

The computational complexity of the Lubich/collocation method is essentially given by that of the construction of the $N+1$ matrices $\bar{\mathbf{A}}_n \in \mathbb{R}^{(M+1)\times(M+1)}$ in (43), and of the evaluation of the volume integral terms. These latter are at most $3N(M+1)$.

Thus, denoting by n_m the number of nodes of the Gauss-Legendre rule used to compute the matrix elements, and recalling that all the matrix elements are computed using the FFT with $L = 2N$ terms, the construction of all matrices is (approximately) defined by that of $2n_m NM^2$ (complex and composite, see (46)) function evaluations. We have also taken into account the special form of the kernel $\bar{K}$ defining the matrix elements (see (47)), and the decomposition strategy we have proposed to treat it. Our (rough) count does not include however, many other (minor) computational issues.

If we denote by n_v the number of points of the quadrature rules presented above, that we will use to compute the volume integrals, then the cost of all volume integrations is given by $2n_v^2(n_v+2)MN$ (real) function evaluations.

To determine the volume integration overhead, we have derived a very rough estimate, given only in terms of real function evaluations. This is:

$$\frac{n_v^2(n_v+2)}{16n_mM} = O(M^{-1}), \tag{55}$$

It represents also an estimate of the overhead associated with the evaluation of the potential at a given point of the PDE space domain, for all $t_n \in (0, T]$.

Thus, for example, when $n_v \approx n_m$ and M is greater than n_v^2, the overhead can be considered negligible. For instance, in Example 4 of the next section, for $T = 1$ we take $n_m = 8$ and $n_v = 12$; therefore, starting from $M = 16$ the above ratio is less than 1 and tends to zero as M increases. We ought however to notice that when the volume integrand functions have a nasty behavior (this happens in our Examples 3 and 4 when T is not small; for instance for $T = 32, 100$), the number of quadrature nodes n_v one has to take is not any longer small. In this case the above overhead can take a significant value, unless the value of M is large enough (see the first case in Example 3), or one can construct ad hoc quadrature rules which require a (significantly) lower number of points.

The numerical testing we will present in the next section shows that estimate (55) is actually too pessimistic.

Finally, we ought to remark that in the above overhead estimates we have assumed to use the same quadrature rules for all time instants $t_n \in [0, T]$. This means that the number of nodes n_v is determined by the accuracy we require in particular at T. But the same accuracy is achieved, for example, at the initial instants by taking a significantly smaller number of nodes, in particular when T is moderate/large. This aspect needs to be further investigated.

4 Numerical examples

Since no theoretical results are known on the stability and convergence of the Lubich/collocation method described in the previous section, as well as for the associated Lubich/Galerkin method, in this section we perform some numerical testing on these properties by considering a few simple examples. We recall that the space approximant we have chosen is a continuous piecewise linear function associated with the chosen (uniform) mesh. At the same time, we will also test the efficiency of the quadrature formulas we have proposed to compute the volume integrals. In the case of fully homogeneous problems we will consider both approaches (33) and (45).

Remark 4.1 *In the collocation case, the elements of the matrix $\bar{\mathbf{A}}_0$ in (45), the only one that needs to be "inverted", are given by*

$$(\bar{\mathbf{A}}_0)_{mi} = \int_{x_0}^{x_{M+1}} \omega_0(\Delta_t; \|\boldsymbol{\psi}(x_m) - \boldsymbol{\psi}(y)\|) N_i(y) |\boldsymbol{\psi}'(y)| dy,$$

where, having set $r_m = \|\boldsymbol{\psi}(x_m) - \boldsymbol{\psi}(y)\|$, we have

$$\omega_0(\Delta_t; r_m) = \frac{\partial^2}{\partial \mathbf{n_x} \partial \mathbf{n_y}} \frac{1}{2\pi} K_0\left(\frac{3}{2}\frac{r_m}{\Delta_t}\right) = \frac{\partial^2}{\partial \mathbf{n_x} \partial \mathbf{n_y}} \frac{\imath}{4} H_0^{(1)}\left(\imath \frac{3}{2}\frac{r_m}{\Delta_t}\right),$$

$K_0(z)$ being the modified Bessel function of the second kind of order 0, and $H_0^{(1)}(z)$ is the zero order Hankel function of the first kind (see [1], (9.6.4)). Therefore $\bar{\mathbf{A}}_0$ is a collocation matrix for the double-layer BIE representation of the Neumann problem for the Helmholtz equation $\triangle u - s^2 u = 0$, with wavenumber $s = 3/(2\Delta_t)$, defined on the

(closed and parametrized) curve Γ. *A similar remark applies also to the corresponding Galerkin matrix.*

The mapping properties of the above mentioned double-layer representations, as well as the behaviors of the corresponding classical Galerkin and collocation matrices, have been known for many years. For the collocation case see, for example [6], [7], [8], [14]. In all the testing we have performed, where we simultaneously let $\Delta_t \to 0$ *and* $M \to \infty$, *the (spectral) condition numbers of the matrices* $\frac{1}{2}\mathbf{I} + \mathbf{A_0}$ *and* $\bar{\mathbf{A}}_0$ *have taken values close to* 1. *Thus, in the cases we have examined the final linear systems one has to solve appear to be very well-conditioned. This seems to be due to the property that the coefficient* $\omega_0(\Delta_t; r_m)$, *which is defined in terms of modified Bessel functions of the second kind* K_0 *and* K_1, *contains (see 9.7.2 in [1]) the factor* $e^{-\frac{3}{2}\frac{r_m}{\Delta t}}$.

We recall that in the 3D case, having denoted by Δ_x the size of the mesh elements of the boundary Γ, for the corresponding Galerkin method the (unconditional) convergence rate forecasted by (18) for regular meshes is, in the (space) $H^{1/2}$-norm, $O(\Delta_t^2) + O(\Delta_x^{3/2})$, uniformly with respect to $t_n \in [0, T]$. Although a similar result has not been derived for the 2D case, this bound would suggest to take Δ_t and Δ_x such that $\Delta_t^2 \approx \Delta_x^{3/2}$, that is,

$$M \approx (b-a)\left(\frac{N}{T}\right)^{4/3}, \ N \to \infty. \tag{56}$$

This criteria has been adopted, for example, in [11]. In such a case the "global order of convergence" should behave like N^{-2}. Otherwise, by taking for example $M = N$ or $M = N/2$, the behavior of the above error would be defined by $N^{-3/2}$. However, for simplicity, in our numerical testing, to examine the convergence behavior of the proposed numerical methods, we have preferred to compute the (space) L^2-norm of the errors. In this case, since in the following examples we perform only uniform partitions of the boundary Γ, it appears reasonable to expect a global rate of convergence of the type $O(\Delta_t^2) + O(\Delta_x^2)$.

Thus in the following examples we will apply our collocation and the associated Galerkin methods and verify if the expected quadratic rate of (unconditional) convergence holds. Since the above convergence estimate is uniform with respect to $t_n \in [0, T]$, we will examine the time pointwise behavior of the space L^2-norm of the errors produced by the proposed methods at the chosen instants t_n.

We will consider four cases: two fully homogeneous and two with non homogeneous data. Two with initial/boundary conditions satisfying the smoothness and compatibility conditions required by the Lubich's theory (Examples 1, 3), and two having data not satisfying all the required compatibility conditions: in Example 2, the first condition (of order 0) is violated, while in Example 4 it is the one of highest order (3) which is not satisfied. In Example 1 we will also consider a domain with corners.

In the numerical testing we present next, all the matrix elements have been computed by applying the n-point Gauss-Legendre rule to each boundary element where the integrand is not identically equal to zero, with $n = 8$ when $T = 1$ and $n = 16$ for the cases $T = 32, 12\pi, 100$. In all tables and figures, we will denote by L/NC, L/SC and L/Gal, the Lubich/nodal collocation, Lubich/shifted collocation and Lubich/Galerkin BEM methods, respectively. Here and in the following, by shifted collocation method we mean the ϵ-collocation method with $\epsilon = 1/3$. There are no special reasons for

choosing this value. As we shall shortly remark, any value not too close to one of the values $0, 1/2, 1$ would be an equally good choice.

Example 1

The first example we have considered is the 2D Neumann problem (1) or (2), with the following homogeneous data:

$$u_0(\mathbf{x}) = 0, \quad v_0(\mathbf{x}) = 0, \quad f(\mathbf{x}, t) = 0, \quad g(\mathbf{x}, t) = -t^4 \exp(-t), \ \mathbf{x} \in \Gamma \tag{57}$$

$t \in [0, T]$ and Γ coinciding with the boundary of the unit disc, parameterized by $\mathbf{x} = \boldsymbol{\psi}(\theta) = (\cos\theta, \sin\theta)$, $\theta = [-\pi, \pi)$. The time interval has been divided into N steps of equal length, and the θ interval into M equal parts (see Section 3.1). In this case, besides the Lubich/collocation method we have also applied the corresponding Lubich/Galerkin method. Notice that the data smoothness and compatibility conditions required to obtain the optimal rate of convergence proved in [11] for the 3D analogue are satisfied.

In the case of the BIEs (19) and (20), to compute the space integrals on their right-hand side, we have first split the parametrization interval in the two subintervals defined by the collocation point and introduced the q-smoothing polynomial transformation defined immediately after (41), with $q = 3$. Then, we have applied to each subinterval the n-point Gauss-Legendre quadrature rule, with $n = 128$ for $T = 1$ and $n = 16$ for $T = 32$ and $T = 12\pi$.

At a first glance such a high number of nodes when $T = 1$ may appear surprising, in particular if compared with that of the case $T = 32$. However, a more careful look at the behavior of the integrand function shows, in the first case, an exponential decay away from interval split point. This phenomenon, which is due to the very small values that the step $\triangle_t$ takes when N is not small, is not significant when $T = 32$. Notice that the choice $n = 128$ when $T = 1$ may be excessively high for the lower values of N. We have made such choice for all values of N only for simplicity reasons.

Since an analytic expression of the exact solution of the above BIEs is not known, to determine the estimated errors for the approximation of $[u(\mathbf{x}, t)] = u^i(\mathbf{x}, t) - u^e(\mathbf{x}, t)$ we have taken as reference solution the approximant given by the chosen Lubich/shifted collocation method applied to the BIE (21) with, taking into account (56), $M = 512, N = 1024$ when $T = 1$, and $M = 256, N = 1024$ for $T = 32$. All the matrix elements have been computed using a 64-point Gauss-Legendre rule.

The approximations of $[u(x, t)]$ obtained by the Lubich/nodal collocation BEM applied to (19)-(20) and by the Lubich/ϵ-collocation applied to (21) are very similar. In Figure 4 we have plotted $[u(x, t)]$ as the function: $(\theta, t) \to \varphi((\cos\theta, \sin\theta), t)$, taking $T = 1$ and $M = 128$, $N = 64$.

In all the tables of Example 1, we have reported the L^2-norm relative errors ($err(t_n) = err_{M,N}(t_n)$), together with the associated estimated orders of convergence (EOC=EOC(t_n), obtained at the intermediate instants $t_n = T/4, T/2, 3T/4$ and at $t_N = T$. These orders have been computed using the standard formula:

$$\text{EOC} = \log_2 \left(err_{M,N}(t_n) / err_{2M,2N}(t_n) \right).$$

We remark that if in the case reported in the last line of Table 2 we take a higher number of quadrature nodes to compute the right hand side space integral, for example $n = 256$, we obtain EOC=2.3 for each time instant.

Figure 4: Example 1. Approximations of $[u(x,t)]$, obtained by L/SC applied to (21); $M = 128, N = 64$. Disc (left-side) and ellipse (right-side) cases

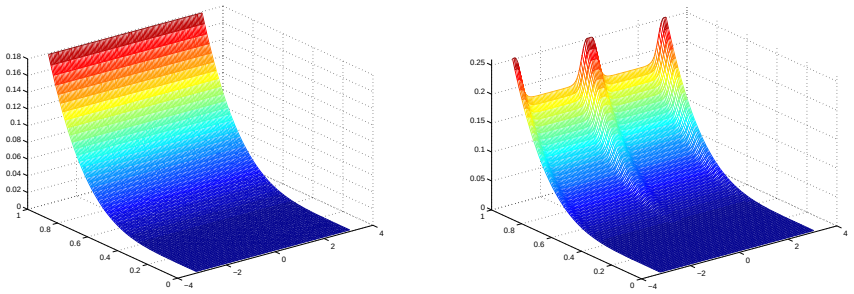

In Tables 3, 4 and 6 we have also reported the 2-norm condition number CN of the matrix $\bar{\mathbf{A}}_0$ (see system (43)) corresponding to the Lubich/collocation BEM used. The condition numbers of the matrix $1/2\mathbf{I} + \mathbf{A}_0$ arising from the discretization of (19) by the Lubich/collocation BEM (see (32)) and of $-1/2\mathbf{I} + \mathbf{A}_0$ for (20) are both less than 1.02 for all the couples of M and N considered.

Table 2: Example 1: $err(t_n)$ and EOC obtained by L/NC applied to (19)-(20). $T = 1$

M	N	$err(T/4)$	EOC	$err(T/2)$	EOC	$err(3T/4)$	EOC	$err(T)$	EOC
8	16	$2.46e-01$		$6.85e-02$		$3.01e-02$		$1.62e-02$	
			1.73		1.85		1.91		1.94
16	32	$7.42e-02$		$1.90e-02$		$8.01e-03$		$4.23e-03$	
			1.84		1.93		1.96		1.98
32	64	$2.06e-02$		$4.98e-03$		$2.05e-03$		$1.07e-03$	
			1.93		1.97		1.99		1.99
64	128	$5.42e-03$		$1.27e-03$		$5.19e-04$		$2.69e-04$	
			2.02		2.04		2.04		2.02
128	256	$1.33e-03$		$3.08e-04$		$1.26e-04$		$6.63e-05$	
			2.23		2.05		1.81		1.57
256	512	$2.85e-04$		$7.42e-05$		$3.59e-05$		$2.23e-05$	

Notice (see Table 3) that in the case of the (standard) collocation method, i.e. $\epsilon = 0$, applied to the hypersingular equation (21), when we take $N = 2M$, a severe instability soon appears as N increases. This behavior does not show up when we take any value of $0 < \epsilon < 1$, $\epsilon \neq 1/2$, although the condition number of $\bar{\mathbf{A}}_0$ increases as ϵ approaches the value $1/2$ (significantly only in a very small neighborhood of this value). Apparently when $\epsilon = 1/2$, in this example the matrix $\bar{\mathbf{A}}_0$ becomes singular. We expect that the values of ϵ for which we have stability do not depend on the shape of the space domain boundary Γ; this because the hypersingularity in (52) lies in the parameter interval, hence it does not depend on the parametrization function. This latter is inserted in the smooth part of the integrand function; thus it could have some effects only on the number of quadrature nodes needed to achieve the required accuracy.

To test this statement, in this example we have replaced the disc by the ellipse $\mathbf{x} = \boldsymbol{\psi}(\theta) = (5\cos\theta, 0.5\sin\theta), \theta \in [-\pi, \pi]$. The corresponding shifted collocation BIE solution, for $T = 1$, has been reported in Figure 4 above. The relative errors produced by the method in this case are very similar to those we have obtained for the disc.

Table 3: Example 1: $err(t_n)$, EOC and CN obtained by L/NC applied to (21). $T = 1$

M	N	CN	$err(T/4)$	EOC	$err(T/2)$	EOC	$err(3T/4)$	EOC	$err(T)$	EOC
4	8	1.2	$7.53E-01$		$2.29E-01$		$1.07E-01$		$5.96E-02$	
				1.61		1.74		1.83		1.88
8	16	1.3	$2.46E-01$		$6.85E-02$		$3.01E-02$		$1.62E-02$	
				1.73		1.85		1.91		1.93
16	32	1.3	$7.42E-02$		$1.90E-02$		$8.03E-03$		$4.24E-03$	
				1.84		1.93		1.96		1.97
32	64	1.4	$2.07E-02$		$5.00E-03$		$2.07E-03$		$1.08E-03$	
				1.93		1.98		1.99		1.99
32	128	1.2	$5.43E-03$		$1.27E-03$		$5.22E-04$		$2.72E-04$	
				2.02		2.03		2.03		2.03
32	256	1.1	$1.34E-03$		$3.11E-04$		$1.28E-04$		$6.68E-05$	
64	128	1.5	$5.43E-03$		$1.27E-03$		$5.21E-04$		$4.20E-01$	
128	256	1.7	$1.33E-03$		$1.15E+04$		$1.54E+17$		$4.10E+30$	

In the testing we have performed, in this example as well as in the following ones, taking $M = 2N$, or $M = N$, or $M = N/2$ or the choice defined in (56), for the values of T and N considered, the ϵ $(= 1/3)$ method, and that defined by any other choice of $0 < \epsilon < 1, \epsilon \neq 1/2$, did not show any instability phenomenon.

Table 4: Example 1: $err(t_n)$, EOC and CN obtained by L/SC applied to (21). $T = 1$

M	N	CN	$err(T/4)$	EOC	$err(T/2)$	EOC	$err(3T/4)$	EOC	$err(T)$	EOC
8	16	2.9	$2.46e-01$		$6.86e-02$		$3.01e-02$		$1.62e-02$	
				1.73		1.85		1.91		1.94
16	32	2.9	$7.42e-02$		$1.90e-02$		$8.02e-03$		$4.24e-03$	
				1.84		1.93		1.96		1.97
32	64	2.9	$2.07e-02$		$5.00e-03$		$2.07e-03$		$1.08e-03$	
				1.93		1.98		1.99		2.00
64	128	2.9	$5.43e-03$		$1.27e-03$		$5.19e-04$		$2.69e-04$	
				2.03		2.05		2.07		2.09
128	256	2.9	$1.33e-03$		$3.06e-04$		$1.24e-04$		$6.31e-05$	
				2.30		2.34		2.43		2.66
256	512	2.9	$2.69e-04$		$6.03e-05$		$2.29e-05$		$1.00e-05$	

To show that our numerical approach is equally efficient also for larger values of T, we have applied the Lubich/collocation BEM taking $T = 32$. The corresponding relative errors are reported in Tables 5 and 6.

The condition numbers of the matrices $1/2\mathbf{I} + \mathbf{A}_0$ for (19) and $-1/2\mathbf{I} + \mathbf{A}_0$ for (20) are less than $1.7E + 00$ and $5.6E + 01$, respectively, for all the couples of M and N considered.

For $T = 32$, the L^2-relative errors of the approximations of $[u(x,t)]$ obtained by applying the Lubich/nodal collocation BEM to (21) with $M = 8$ fixed, to avoid the above mentioned instability phenomena, and with increasing values of N, using 16 quadrature nodes for each matrix entry, are quite similar to those obtained by the Lubich/shifted collocation BEM. Therefore, in Table 6 we have reported only these latter. As for the corresponding condition numbers, the values of CN given by the Lubich/nodal collocation BEM are similar to those reported in Table 6.

We remark that the matrix elements have been computed by applying the numerical procedure described in Section 3.1, which takes into account the behavior of the involved Bessel functions and prevents possible numerical cancelation phenomena.

Table 5: Example 1: $err(t_n)$ and EOC obtained by L/NC applied to (19)-(20). $T = 32$

M	N	$err(T/4)$	EOC	$err(T/2)$	EOC	$err(3T/4)$	EOC	$err(T)$	EOC
4	16	$8.55e-02$		$8.31e-03$		$6.30e-03$		$5.93e-03$	
			2.38		6.80		5.60		5.64
8	32	$1.64e-02$		$7.47e-05$		$1.30e-04$		$1.19e-04$	
			2.30						
16	64	$3.34e-03$		$1.53e-04$		$1.52e-04$		$1.45e-04$	
			2.15		1.28		1.12		1.03
32	128	$7.53e-04$		$6.33e-05$		$7.00e-05$		$7.10e-05$	
			2.22		0.92		0.42		0.46
64	256	$1.61e-04$		$3.34e-05$		$5.24e-05$		$5.15e-05$	
			1.96		0.27		1.10		0.59
128	512	$4.15e-05$		$2.78e-05$		$2.45e-05$		$3.42e-05$	

Table 6: Example 1: $err(t_n)$, EOC and CN obtained by L/SC applied to (21). $T = 32$

M	N	CN	$err(T/4)$	EOC	$err(T/2)$	EOC	$err(3T/4)$	EOC	$err(T)$	EOC
4	16	1.9	$8.59e-02$		$8.64e-03$		$6.58e-03$		$6.18e-03$	
				2.34		4.86		5.18		5.26
8	32	1.6	$1.70e-02$		$2.98e-04$		$1.82e-04$		$1.61e-04$	
				2.23		3.14		5.25		5.46
16	64	1.6	$3.61e-03$		$3.37e-05$		$4.76e-06$		$3.67e-06$	
				2.05		0.56		1.54		
32	128	1.6	$8.74e-04$		$2.29e-05$		$1.64e-06$		$6.64e-06$	
				1.86				0.02		0.29
64	256	1.6	$2.41e-04$		$2.78e-05$		$1.62e-06$		$5.41e-06$	
				2.72		0.88				1.65
128	512	1.6	$3.66e-05$		$1.52e-05$		$1.12e-05$		$1.72e-06$	

We have compared the elapsed time required to solve equations (19) and (21), using the Lubich/nodal collocation and the Lubich/shifted BEM method, respectively, when $T = 32$. The hypersingular equation approach is faster. Indeed, if we consider the case $T = 32$, which is the one more favorable to (19), and we take $M = 4, 8, 16, 32, 64, 128$ ($N = 4M$), the corresponding computational times required by the two methods are $0.5, 2.5, 15.2, 98.2, 679.9, 4.9E3$ and $0.4, 1.8, 10.5, 67.1, 454.6, 3.1E3$ seconds, respectively. We recall that, while the total CPU time needed for the solution of (21) is essentially given by the construction of the linear system matrices, about 3/4 of that required for the solution of (19) is devoted to the known term computation. For this reason, when $T = 1$, the comparison is even more favorable to formulation (21). This computational difference is further amplified when one then compute the associated potential at the required points.

For the ellipse domain we have previously considered, also in the case $T = 32$ the ϵ-collocation method has produced results very similar to those we have obtained above for the disc.

In Tables 7 and 8 we have reported the corresponding errors for $T = 1$ and $T = 32$ respectively, obtained by the Lubich/Galerkin BEM. All integrals needed to construct Table 8 have been obtained using a 25×24-point tensor product Gauss-Legendre rules.

As we can see, the Lubich/Galerkin BEM has produced numerical results very similar to those given by the Lubich/shifted collocation BEM. Nevertheless, it has to be mentioned that the numerical results in Tables 7 and 8 have been obtained by using appropriate quadrature formulas, which take into account the (boundary or internal) position of the hypersingularity with respect to the domain of integration. Moreover, in

Tables 7 and 8 the matrix entries have been computed by using 9×8 and 17×16 tensor product Gaussian rules, respectively, after having introduced, whenever needed, a q-smoothing transformation. Therefore, the computation of the matrix entries is quite delicate and expensive, and the overall computation is by far more time consuming than that of the corresponding collocation method.

Table 7: Example 1: $err(t_n)$, EOC and CN obtained by L/Gal applied to (21). $T = 1$

M	N	CN	$err(T/4)$	EOC	$err(T/2)$	EOC	$err(3T/4)$	EOC	$err(T)$	EOC
8	16	2.9	$2.56e-01$		$7.34e-02$		$3.33e-02$		$1.86e-02$	
				1.74		1.85		1.90		1.93
16	32	2.9	$7.68e-02$		$2.03e-02$		$8.91e-03$		$4.90e-03$	
				1.84		1.92		1.95		1.96
32	64	2.9	$2.14e-02$		$5.37e-03$		$2.31e-03$		$1.26e-03$	
				1.93		1.97		1.98		1.97
64	128	2.9	$5.62e-03$		$1.37e-03$		$5.86e-04$		$3.20e-04$	
				2.02		2.02		1.98		1.89
128	256	3.0	$1.39e-03$		$3.37e-04$		$1.49e-04$		$8.63e-05$	
				2.26		2.11		1.75		1.25
256	512	3.0	$2.90e-04$		$7.84e-05$		$4.40e-05$		$3.62e-05$	

Table 8: Example 1: $err(t_n)$, EOC and CN obtained with L/Gal applied to (21). $T = 32$

M	N	CN	$err(T/4)$	EOC	$err(T/2)$	EOC	$err(3T/4)$	EOC	$err(T)$	EOC
4	16	2.1	$8.86e-02$		$1.06e-02$		$8.47e-03$		$8.04e-03$	
				2.35		4.18		4.21		4.22
8	32	1.4	$1.74e-02$		$5.86e-04$		$4.56e-04$		$4.31e-04$	
				2.24		2.82		3.09		3.23
16	64	1.2	$3.67e-03$		$8.28e-05$		$5.37e-05$		$4.60e-05$	
				2.05		1.26		1.87		2.42
32	128	1.2	$8.85e-04$		$3.46e-05$		$1.47e-05$		$8.61e-06$	
				1.86		0.10		1.38		0.47
64	256	1.2	$2.44e-04$		$3.22e-05$		$5.65e-06$		$6.21e-06$	
				2.69		0.74				
128	512	1.2	$3.80e-05$		$1.93e-05$		$2.11e-05$		$1.69e-05$	

We have compared the computational time required by the ϵ-collocation and the Galerkin methods, in particular for the construction of their associated matrices, taking into account the symmetry of the Galerkin matrix blocks $\mathbf{A}_n$, but not that of those of the collocation method, which depends on the shape of the boundary Γ. To generate each approximation reported in the tables above, the CPU time required by the Galerkin approach has been about 35 times that needed by the ϵ-collocation method.

In the last four tables we notice that an error barrier appears as soon as the maximum accuracy (of order $10^{-5} \div 10^{-6}$) the method can produce is achieved. This is probably due to the evaluation of the Lubich ω coefficients by means of the quadrature (34), with parameters defined by (35). Moreover, we ought to remark that we do not compute these coefficients explicitly, since, to speed up the overall computation, the FFT algorithm is applied to the trapezoidal sum in (46) after having computed the integrals over (x_0, x_{M+1}). Thus also the quadrature rules used to evaluate the latter (space) integrals come into play. This aspect of the numerical solution method needs further investigation, in particular if one has to solve the problem with higher accuracy. Nevertheless, we remind that the errors we have computed are pointwise, with

respect to the time instant t_n, while estimate (18) is uniform in $[0, T]$. In particular, for $T = 32$ the largest absolute errors are produced at values t_n much smaller than T; in our tables this happens at $t_n = T/4$.

We have also applied the above Lubich/ϵ-collocation method to the problem defined by the conditions (57), but with the Neumann boundary data replaced by

$$g(x, t) = -t^4 \exp(-(x_1^2 + 2x_2^2)).$$

The corresponding results are reported in Tables 9 and 10, where the new problem is identified as Example 1bis.

Table 9: Example 1bis: $err(t_n)$, EOC and CN obtained by L/SC applied to (21). $T = 1$

M	N	CN	$err(T/4)$	EOC	$err(T/2)$	EOC	$err(3T/4)$	EOC	$err(T)$	EOC
16	4	2.4	$2.36e+00$		$8.23e-01$		$4.40e-01$		$2.81e-01$	
				1.55		1.62		1.68		1.72
32	8	2.4	$8.07e-01$		$2.68e-01$		$1.38e-01$		$8.53e-02$	
				1.61		1.72		1.78		1.81
64	16	2.4	$2.64e-01$		$8.15e-02$		$4.01e-02$		$2.44e-02$	
				1.73		1.84		1.87		1.86
128	32	2.4	$7.94e-02$		$2.28e-02$		$1.09e-02$		$6.71e-03$	
				1.90		1.97		1.96		1.90
256	64	2.4	$2.13e-02$		$5.83e-03$		$2.81e-03$		$1.80e-03$	
				2.23		2.26		2.22		2.10
512	128	2.4	$4.52e-03$		$1.22e-03$		$6.06e-04$		$4.22e-04$	

Table 10: Example 1bis: $err(t_n)$, EOC and CN obtained by L/SC applied to (21). $T = 100$

M	N	CN	$err(T/4)$	EOC	$err(T/2)$	EOC	$err(3T/4)$	EOC	$err(T)$	EOC
4	16	11.4	$7.12e-01$		$1.93e-01$		$7.80e-02$		$3.37e-02$	
				1.68		1.57		1.35		0.94
8	32	6.1	$2.23e-01$		$6.50e-02$		$3.05e-02$		$1.76e-02$	
				1.82		1.89		1.92		1.93
16	64	3.8	$6.30e-02$		$1.75e-02$		$8.08e-03$		$4.62e-03$	
				1.91		1.96		1.97		1.98
32	128	2.8	$1.68e-02$		$4.52e-03$		$2.06e-03$		$1.17e-03$	
				2.01		2.04		2.05		2.05
64	256	2.6	$4.17e-03$		$1.10e-03$		$4.97e-04$		$2.82e-04$	
				2.29		2.30		2.31		2.31
128	512	2.5	$8.54e-04$		$2.23e-04$		$1.00e-04$		$5.67e-05$	

Finally, to check further the performance of the proposed Lubich/shifted collocation BEM, we have solved the problem of this example taking, however, a domain with corners: the square with vertices at $(\pm 1, 0), (0, \pm 1)$. The corresponding results have been reported in Figure 5 and in Table 11. A comparison of this latter table with Table 4 indicates a loss of accuracy: the order of convergence appears to be close to 3/2.

Figure 5: Example 1: approximation of $[u(x,t)]$, obtained by L/SC applied to (21); $M = 128, N = 64$.

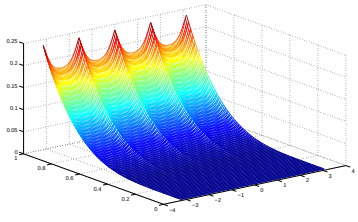

Table 11: Example 1: $err(t_n)$, EOC and CN obtained by L/SC applied to (21). $T = 1$

M	N	CN	$err(T/4)$	EOC	$err(T/2)$	EOC	$err(3T/4)$	EOC	$err(T)$	EOC
8	16	3	$2.26e-01$		$7.59e-02$		$6.32e-02$		$5.29e-02$	
				1.54		0.64		0.87		1.10
16	32	3	$7.77e-02$		$4.87e-02$		$3.45e-02$		$2.47e-02$	
				0.98		1.33		1.41		1.25
32	64	3	$3.93e-02$		$1.94e-02$		$1.30e-02$		$1.04e-02$	
				1.42		1.35		1.22		1.21
64	128	3	$1.47e-02$		$7.59e-03$		$5.58e-03$		$4.49e-03$	
				1.52		1.33		1.33		1.27
128	256	3	$5.14e-03$		$3.02e-03$		$2.22e-03$		$1.86e-03$	
				1.67		1.66		1.64		1.31
256	512	3	$1.62e-03$		$9.54e-04$		$7.12e-04$		$7.52e-04$	

Example 2

As Example 2 we have considered the following 2D Neumann problem with homogeneous data, but with a boundary condition that does not satisfy all the smoothness and compatibility conditions, at $t = 0$, required by the theory developed in [11] for the 3D case, to guarantee the convergence:

$$u_0(\mathbf{x}) = 0, \quad v_0(\mathbf{x}) = 0, \quad f(\mathbf{x},t) = 0, \quad g(\mathbf{x},t) = H(t), \ \mathbf{x} \in \Gamma \tag{58}$$

$t \in [0, 12\pi]$ and Γ coinciding with the boundary of the unit disc. This test problem has been already considered in [5] and in [2].

In Figure 6, on the left we have plotted the time history of the approximate solution $u^e(A,t)$ at the point $A = (0,1)$ of Γ; the corresponding approximation of $[u(A,t)] = u^i(A,t) - u^e(A,t)$ is reported on the right hand side. These curves have been obtained by applying the Lubich/nodal collocation method to (19),(20) (dashed line), and by solving the BIE (21) by means of the Lubich/shifted collocation method (dotted line). For both methods we have chosen $M = 32$ and $N = 16$. The graphs of the two curves overlap.

In Tables 12 and 13, we have reported the L^2-norm relative errors and the experimental convergence orders, obtained at the intermediate instants $t_n = T/4, T/2, 3T/4$ and at $t_N = T = 12\pi$. As reference solution we have taken the approximant given by the chosen Lubich/ϵ-collocation method applied to the BIE (21) with $M = 256, N = 1024$; the associated matrix elements have computed using the 64-point Gauss-Legendre rule.

In Table 12, to compute the q-transformed right hand side integrals, with $q = 3$, we have applied the 16-point Gauss-Legendre quadrature.

Figure 6: Example 2: approximations of $u^e(A,t)$ (on the left) and $[u(A,t)]$ (on the right), obtained by L/NC applied to (19)-(20) (dashed line) and by L/SC applied to (21) (dotted line), with $M = 32, N = 16$.

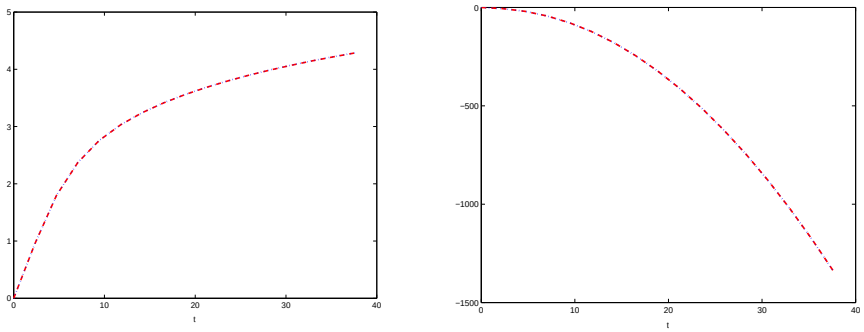

Table 12: Example 2: $err(t_n)$ and EOC obtained by L/NC BEM applied to (19)-(20), $T = 12\pi$

M	N	$err(T/4)$	EOC	$err(T/2)$	EOC	$err(3T/4)$	EOC	$err(T)$	EOC
4	16	$1.52e-01$		$9.95e-02$		$7.15e-02$		$5.58e-02$	
			0.66		0.86		0.92		0.94
8	32	$9.64e-02$		$5.50e-02$		$3.78e-02$		$2.90e-02$	
			0.88		0.97		1.00		1.01
16	64	$5.23e-02$		$2.82e-02$		$1.89e-02$		$1.44e-02$	
			1.01		1.04		1.09		1.09
32	128	$2.59e-02$		$1.37e-02$		$8.87e-03$		$6.76e-03$	
			1.15		1.16		1.23		1.22
64	256	$1.17e-02$		$6.09e-03$		$3.78e-03$		$2.91e-03$	
			1.79		1.35		1.62		1.66
128	512	$3.37e-03$		$2.40e-03$		$1.23e-03$		$9.21e-04$	

For (19) and (20) the 2-norm condition numbers of the matrices $1/2\mathbf{I} + \mathbf{A}_0$ and $-1/2\mathbf{I} + \mathbf{A}_0$ are less than 1.9 and 7.4, respectively, for all the couples of values of M and N considered.

As for Example 1, the relative errors obtained by the Lubich/Galerkin BEM are comparable with those given by the Lubich/shifted collocation BEM. For this reason we have omitted them.

We remark that in this example the required compatibility conditions are not all satisfied. In particular we have $g(\mathbf{x}, 0^+) = 1 \neq \frac{\partial u_0(\mathbf{x})}{\partial \mathbf{n}} = 0$. Nevertheless, the method appears to be convergent, with a convergence rate which seems to move toward 2 as M, N increase.

Example 3

As an example of a 2D exterior Neumann problem (1) with non homogeneous, smooth and compatible data according to Remark 2.7 and the following statements, we have first considered the following problem:

$$\begin{aligned} &u_0(\mathbf{x}) = \exp(-(x_1+x_2)^2),\ v_0(\mathbf{x}) = 2\sqrt{2}(x_1+x_2)\exp(-(x_1+x_2)^2),\\ &f(\mathbf{x},t) = 0,\\ &g(\mathbf{x},t) = 2(x_1+x_2-\sqrt{2}t)(x_1+x_2)\exp(-(x_1+x_2-\sqrt{2}t)^2),\ \mathbf{x} = (x_1,x_2) \in \Gamma \end{aligned} \tag{59}$$

$t \in [0,T]$ and Γ coinciding with the boundary of the unit disc. The exact solution of this problem is the plane progressive wave $u(\mathbf{x},t) = \exp(-(x_1+x_2-\sqrt{2}t)^2)$. Since

Table 13: Example 2: $err(t_n)$, EOC and CN obtained by L/SC applied to (21). $T = 12\pi$

M	N	CN	$err(T/4)$	EOC	$err(T/2)$	EOC	$err(3T/4)$	EOC	$err(T)$	EOC
4	16	2.3	$1.52e-01$		$9.92e-02$		$7.13e-02$		$5.55e-02$	
				0.66		0.86		0.93		0.95
8	32	2.3	$9.59e-02$		$5.46e-02$		$3.75e-02$		$2.87e-02$	
				0.88		0.97		1.01		1.01
16	64	2.3	$5.20e-02$		$2.80e-02$		$1.87e-02$		$1.42e-02$	
				1.01		1.04		1.09		1.09
32	128	2.3	$2.58e-02$		$1.36e-02$		$8.79e-03$		$6.69e-03$	
				1.15		1.17		1.24		1.23
64	256	2.3	$1.16e-02$		$6.04e-03$		$3.73e-03$		$2.86e-03$	
				1.81		1.36		1.65		1.69
128	512	2.3	$3.32e-03$		$2.36e-03$		$1.19e-03$		$8.86e-04$	

this is also the solution of the associated interior problem, in our BIE (15) we ought to have $\varphi(\mathbf{y}, \tau) \equiv 0$.

Figure 7: Example 3, Problem (59): maximum absolute errors, equation (15) known term evaluation. $T = 1, 5, 100; M = 16, N = 32$.

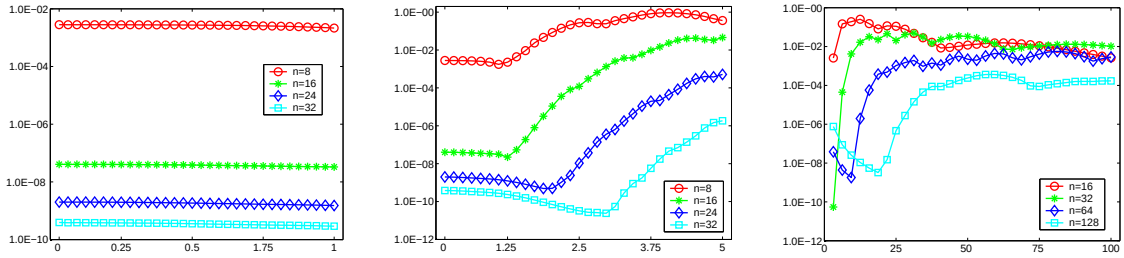

To test the performance of the quadrature rules we have proposed in Section 3.2 to compute the volume integrals, in Figure 7 we have reported, for each of the instants $t_m,\ m = 1 : N(= 32)$, the maximum of the absolute errors obtained at the grid points $(M = 16)$, when we have evaluated the equation known term using n-point basic rules. Since the corresponding L^2-norm errors produced by the Lubich/shifted collocation method are very similar, we have omitted them. We recall however that, since the true solution of our BIE (15) is the null function, the latter errors do not improve as M, N increase. In this particular case, even for small values of M and N the BIE approximant accuracy appears to be determined only by that of the volume integration; the error produced by the Lubich/shifted collocation discretization appears to be negligible. We had the same errors for all choices of M, N we made, in particular for the lowest ones $(M = 16, N = 8)$.

We remark that, with respect to the case $T = 1$, for $T = 5$ the accuracy decreases. The loss of accuracy is even higher when $T = 100$. This because of the behaviors of the functions v_0 in (11) and u_0 in (12). These behaviors have been plotted in Figures 8 and 9, for $T = 5$ and $T = 100$ respectively.
Each function has been considered at $\mathbf{x} = (1, 0)$, first as a function of the variable $\xi \in (0, 1)$, by setting $\theta = \pi$, and then of the variable $\theta \in (0, 2\pi)$ by setting $\xi = 0.5$. Because of these behaviors, for large values of T, to evaluate the integrals I_{v_0} and I_{u_0}

Figure 8: Example 3, Problem (59): v_0 (left-side) and u_0 (right-side). $T = 5$

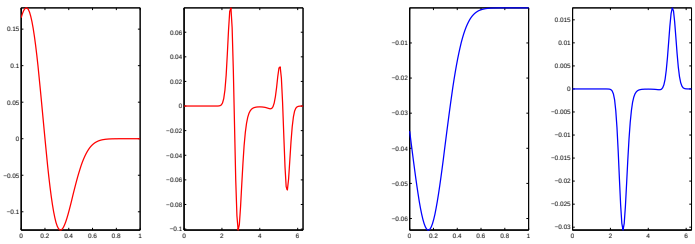

Figure 9: Example 3, Problem (59): v_0 (left-side) and u_0 (right-side). $T = 100$

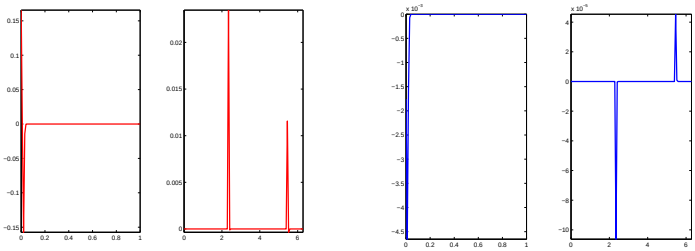

we have to take a sufficiently large value of n, or to use ad hoc quadrature formulas that takes into account the "nasty" behavior of the integrands.

Notice that the error behaviors reported in Figure 7 confirm the last remark we made at the end of Section 3.

To verify the reliability of our volume integration overhead estimate (55), we have solved problem (59) taking for simplicity $N = M = 2^k, k = 3 : 9$, for $T = 1, 5, 100$. For these values of T, the corresponding volume integrations have been performed choosing $n = 16, 32, 128$, respectively. The computation of the matrix elements has been performed using $8, 8, 16$ nodes, respectively. The ratios R_{CPU} between the CPU time required by the computation of all elements of the system right hand sides $\bar{\mathbf{g}}_n, n = 0 : N$, and that of the (simultaneous) computation, by means of the FFT, of the elements of all the matrices $\bar{\mathbf{A}}_{n-j}$ in (43), for $M = [16, 32, 64, 128, 256]$ are $[0.39, 0.16, 0.06, 0.02, 0.008]$ when $T = 1$, $[1.36, 0.53, 0.20, 0.07, 0.03]$ when $T = 5$, and $[13.68, 5.51, 1.48, 0.43, 0.14]$ for $T = 100$, respectively.

To check that the potential does not depend on the chosen extension of the problem data in the whole $\mathbb{R}^2$ space, we have considered problem (59), first with the initial value $u_0(\mathbf{x})$ trivially extended by the the given expression, and then smoothly extended in the interior domain by adding to the previous natural extension the function $\exp(-1/(1 - x_1^2 - x_2^2))$. This latter data is denoted by $\bar{u}_0(\mathbf{x})$. In particular, in Table 14 we have reported the relative errors obtained when computing the potential $u(\mathbf{x}, t)$ at the points $\mathbf{x} = (\sqrt{2}, \sqrt{2})$ and $\mathbf{x} = (3, 0)$, having chosen $T = 1$. In this table, an empty space means that the accuracy obtained at the previous stage remains constant.

We remark that the exceptional accuracy produced in the u_0 case is due to the fact that the associated density function is the zero constant. Thus the relative errors we

Table 14: Example 3, Problem (59): potential relative errors at $\mathbf{x} = (\sqrt{2}, \sqrt{2})$ and at $\mathbf{x} = (3, 0)$ obtained by L/SC applied to (21). $T = 1$

		$\mathbf{x} = (\sqrt{2}, \sqrt{2})$				$\mathbf{x} = (3, 0)$			
		initial data u_0							
M	N	$T/4$	$T/2$	$3T/4$	T	$T/4$	$T/2$	$3T/4$	T
16	8	$9.33E-11$	$9.99E-10$	$6.19E-09$	$3.77E-08$	$4.06E-15$	$3.34E-11$	$4.74E-09$	$1.06E-07$
32	16	$1.05E-13$	$4.91E-11$	$3.28E-09$	$3.51E-08$	$--$			
64	32	$3.57E-15$	$2.26E-11$	$2.59E-09$	$3.33E-08$				
		initial data $\bar{u}_0$							
M	N	$T/4$	$T/2$	$3T/4$	T	$T/4$	$T/2$	$3T/4$	T
16	8	$6.39E-04$	$7.24E-03$	$2.92E-02$	$6.57E-02$	$1.42E-08$	$4.91E-07$	$6.22E-06$	$4.56E-05$
32	16	$1.10E-07$	$5.41E-05$	$2.48E-03$	$2.57E-02$	$6.85E-14$	$3.37E-11$	$4.89E-09$	$1.28E-07$
64	32	$2.02E-14$	$1.47E-08$	$5.79E-05$	$8.24E-03$				
128	64	$--$	$2.25E-11$	$1.14E-07$	$1.96E-03$				
256	128			$2.53E-09$	$2.89E-04$				

have reported in the table are essentially due to the volume integration formulas. This is not the case of the $\bar{u}_0$ data. We further remark that in this second case, also when we have $t = t_n \leq r_{min} = \min_{\mathbf{y}\in\Gamma} \|\mathbf{x}-\mathbf{y}\|$, the potential contribution due to the space-time main integral is negligible, since its theoretical value is zero. As $t > r_{min}$ increases, the above contribution becomes more significant and, from a certain time value on, the global integration error is essentially given by that of the Lubich quadrature.

The results reported in Table 14 have been obtained by using 16-point quadrature rules (32 nodes for the trapezoidal rule) for the volume integration. For $M = [16, 32, 64, 128, 256]$ ($N = M/2$), the corresponding values of the overhead ratio R_{CPU} are $[0.19, 0.08, 0.03, 0.01, 0.001]$.

Another example of a 2D exterior Neumann problem (1), with non homogeneous data and for which the corresponding BIE solution $\varphi(\mathbf{y}, s)$ is identically equal to zero, is:

$$\begin{aligned} &u_0(\mathbf{x}) = \sin(x_1 + x_2),\ v_0(\mathbf{x}) = -\sqrt{2}\cos(x_1 + x_2), \\ &f(\mathbf{x}, t) = 0, \\ &g(\mathbf{x}, t) = -\cos(x_1 + x_2 - \sqrt{2}t)(x_1 + x_2),\ \mathbf{x} = (x_1, x_2) \in \Gamma \end{aligned} \tag{60}$$

$t \in [0, T]$ and Γ coinciding with the boundary of the unit disc. For this example the exact solution of the homogeneous wave equation is the harmonic wave $u(\mathbf{x}, t) = \sin(x_1 + x_2 - \sqrt{2}t)$.

As for the previous case, in Figure 10 we have reported, for each of the instants $t_m,\ m = 1 : N$, the maximum of the absolute errors obtained at the grid points, when we have evaluated the equation known term using n-point basic rules.

By looking at the oscillating behavior of the functions v_0 and u_0 reported in Figures 11 and 12, respectively, the reasons for which the value of n must be chosen larger, as T increases, are evident.

Example 4

Figure 10: Example 3, Problem (60): maximum absolute errors, equation (15) known term evaluation. $T = 1, 5, 100$.

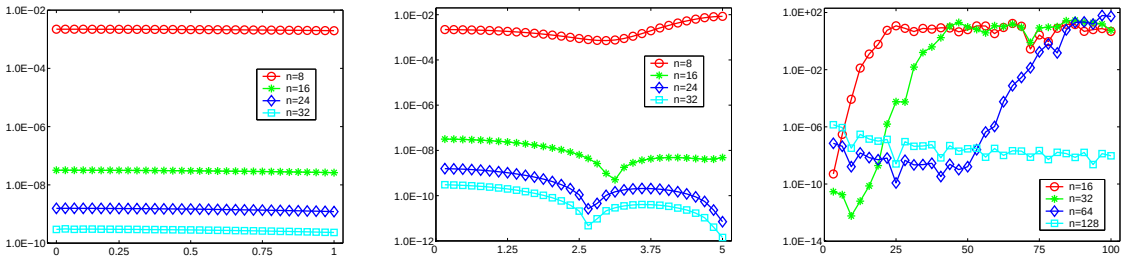

Figure 11: Example 3, Problem (60): v_0 (left-side) and u_0 (right-side). $T = 5$

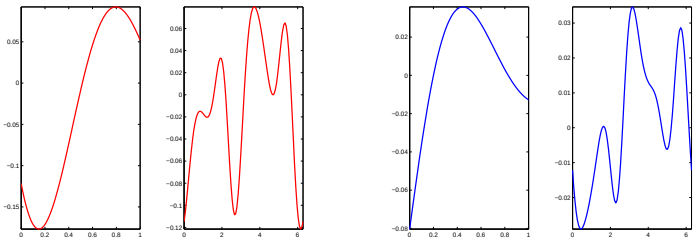

As a last example of a 2D Neumann problem with non homogeneous data, we have considered the one associated with the following smooth data:

$$\begin{aligned} &u_0(\mathbf{x}) = \exp(-(x_1^2 + 2x_2^2)),\ \ v_0(\mathbf{x}) = \exp(-(2x_1^2 + x_2^2)), \\ &f(\mathbf{x}, t) = t^3 \exp(-(x_1^2 + x_2^2)), \\ &g(\mathbf{x}, t) = \frac{\partial u_0}{\partial \mathbf{n_x}} + t\frac{\partial v_0}{\partial \mathbf{n_x}} + \frac{t^2}{2}\frac{\partial}{\partial \mathbf{n_x}}\Delta u_0,\ \ \mathbf{x} = (x_1, x_2) \in \Gamma \end{aligned} \tag{61}$$

$t \in [0, T]$ and Γ coinciding with the boundary of the unit disc.

Notice that in this case we have (see Remark 2.7) $\frac{d^i}{dt^i}\bar{g}(\mathbf{x}, 0) = 0$ only for $i \leq 2$, while the Lubich's theory compatibility condition requires $i \geq 3$. In Figure 13 we have reported the picture of the BIE solution, obtained by using the Lubich/Galerkin BEM.

In Table 15 the volume terms have been computed by using 12 quadrature nodes for each integral. In this table we have also reported the volume integration overhead (R_{CPU} column) defined in Example 3.

The numerical results produced by the Lubich/shifted collocation and Lubich/Galerkin methods are very similar; however the CPU time required by the latter, which is essentially due to the evaluation of the system known term, has been more than 100 times that required by the collocation method. The CPU time required by the program we have written for this latter, to compute simultaneously all the system block matrices and the associated known terms for the values of M, N reported in Table 15, and that we report in the form $(\tau_1 + \tau_2)$, have been $(1.7 + 6.9), (6.7 + 15.1), (31.2 + 35.4), (160.3 + 89.8), (908.1 + 257.4)$, respectively.

Figure 12: Example 3, Problem (60): v_0 (left-side) and u_0 (right-side). $T = 100$

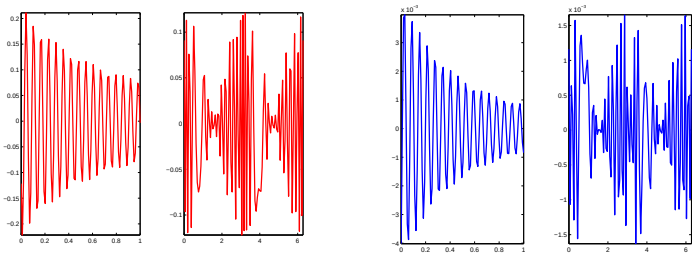

Figure 13: Example 4: approximation of $[u(x,t)]$, obtained by L/Gal applied to (15); $M = 256, N = 128$.

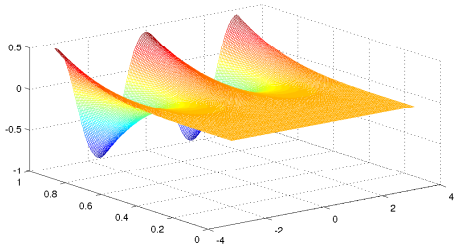

Remark 4.2 *We have also performed some testing on the rate of convergence of our collocation method, when the domain boundary is interpolated by piecewise polynomials on the same mesh used to approximate, by a continuous piecewise linear function, the BIE solution. In particular, taking also into account the results reported in [38], in the previous examples we have interpolated the boundary* Γ *by continuous piecewise linear and quadratic polynomials, and by quadratic and cubic periodic (smooth) splines. In the first two cases the collocation method has shown a first order convergence rate, while in the latter two cases we have obtained error estimates, and corresponding convergence orders, very similar to those we had using the boundary parametric representation. Therefore, it appears that the boundary approximation by a periodic quadratic spline, interpolating the boundary at the mesh midpoints, is sufficient to guarantee a quadratic rate of convergence. We recall that in the Dirichlet case, to obtain the second order*

Table 15: Example 4: $err(t_n)$, EOC and CN obtained by L/SC applied to (15). $T = 1$

M	N	CN	$err(T/4)$	EOC	$err(T/2)$	EOC	$err(3T/4)$	EOC	$err(T)$	EOC	R_{CPU}
16	4	2.3	$1.96e+00$		$6.56e-01$		$3.07e-01$		$1.62e-01$		4.16
				1.58		1.64		1.69		1.68	
32	8	2.4	$6.56e-01$		$2.10e-01$		$9.48e-02$		$5.03e-02$		2.26
				1.65		1.75		1.76		1.62	
64	16	2.4	$2.08e-01$		$6.26e-02$		$2.80e-02$		$1.64e-02$		1.14
				1.84		1.90		1.81		1.60	
128	32	2.4	$5.81e-02$		$1.68e-02$		$7.95e-03$		$5.42e-03$		0.56
				2.28		2.23		2.08		1.87	
256	64	2.4	$1.20e-02$		$3.59e-03$		$1.88e-03$		$1.48e-03$		0.28

convergence rate it was sufficient to interpolate the boundary by a continuous piecewise linear function.

All the numerical computation has been performed on a PC with two Intel Xeon® E5420 (2GHz) processors. We remark, however, that we have not considered the special features of our PC. To perform our numerical testing we have written standard (i.e., sequential) Matlab® codes.

5 Conclusions

The main goal of the paper has been the efficient numerical solution of a hypersingular space-time boundary integral equation associated with Neumann problems for the (in general nonhomogeneous) wave equation, with non trivial initial data. We have assumed that the problem has a classical (smooth) solution. The numerical approach we have examined is one based on a Lubich second order discrete convolution quadrature and on a collocation BEM defined on a uniform mesh. In particular we have examined all the integrals required by the implementation of this method, including those defining the matrices of the associated linear system. For their numerical evaluation we have proposed some simple and efficient rules. Although this calculation is a crucial point for the success of the overall numerical approach, as our intensive numerical testing has shown, it is often ignored or underestimated in the papers written on this topic.

In the case of a 3D Lubich/Galerkin BEM, an unconditionally optimal rate of convergence, uniform with respect to the time instants $t_n \in [0, T]$ and in the $H^{1/2}$-norm with respect to the space variable, has been derived in [11]. A quick look at the theory behind the proof seems to suggest that a similar result should hold also for the corresponding 2D case. For the collocation method we have considered, no (theoretical) stability and convergence results are known. Nevertheless, the numerical testing we have performed in the 2D case seems to indicate that, contrary to the Dirichlet case (see [15]), unconditional stability and convergence, having the same rate of the Galerkin method, hold only for the ϵ-collocation BEM we have considered. This is associated with a uniform mesh of the boundary parametrization interval. For computational simplicity, to measure the convergence rate we have considered the L^2-norm instead of the $H^{1/2}$ one; in this case, our numerical testing seems to confirm a second order convergence rate, with respect to both discretization parameters.

Moreover, although the theory developed in [11] for the 3D Galerkin method requires that the problem data are sufficiently smooth and satisfy some (classical) compatibility conditions, we have applied the proposed Lubich/collocation method, as well as the associated Lubich/Galerkin method, also to problems where the requested conditions are not all satisfied. Like in the Dirichlet case, we have obtained a rate of convergence close to that predicted for "smooth" problems.

In the two non homogeneous examples we have considered, we have also computed the CPU overhead due to the volume integral evaluations. When the final time instant T is fairly small, or, if large, the number of boundary elements M is large enough, this is either negligible or very moderate. Notice that when the BIE solution has a non simple shape, we have necessarily to choose M large to obtain the required accuracy. The dependence of the above overhead on the number of time instants N (see the computational analysis made at the end of Section 3) appears to be negligible. We

remark that in the case of data having a local support this overhead should be even more negligible.

In the testing we have performed, the ϵ-collocation and Galerkin methods produce very similar accuracies; however, the first one is much faster. Unfortunately, this has not a 3D analogue; therefore, at the moment, only the Galerkin method can be used to solve 3D Neumann problems. In this case, the use of fast solution methods is mandatory.

The collocation method cannot be applied also when a data are not sufficiently smooth, to guarantee the continuity of the corresponding volume term, with respect to its variables. This is the case, for example, of a data containing delta Dirac factors, as in the problem treated in [19].

The nodal collocation method, for the solution of 2D and 3D Dirichlet problems, described in [15], and the ϵ-collocation method we have presented in this paper, for the 2D Neumann problem, besides being much faster than the Galerkin counterpart, in the testing we have performed have shown similar accuracies and rates of convergence. Furthermore, the linear systems they give rise are perfectly conditioned. We ought however to remark that the collocation approach has been proposed to solve smooth problems on domains having a smooth boundary. The promising results we have obtained for the collocation approach are also related to the uniform mesh that we have chosen for the boundary parametrization interval. A graded mesh would give rise to a linear system which in general is not well conditioned. But this type of mesh is required only when the solution we are approximating has an irregular behavior, which is not the case we have considered in this paper. In such a situation, the Galerkin approach is certainly more suitable.

Further investigation is thus needed on the performance on the proposed methods, when the data and/or the domain boundary Γ have not the required degree of smoothness. Also the case of data with local supports needs to be investigated further.

Acknowledgement

The authors are grateful to the referees for their stimulating comments

Funding

This work was supported by the Ministero dell'Istruzione, dell'Università e della Ricerca of Italy, under the research program PRIN07: Boundary element methods for time-dependent problems.

References

[1] M. Abramowitz and I. Stegun. *Handbook of Mathematical Functions*. National Bureau of Standards. A.M.S. 55, 1967.

[2] A.I. Abreu, J.A.M. Carrer, and W.J. Mansur. Scalar wave propagation in 2D: a BEM formulation based on the operational quadrature method. *Engineering Analysis with Boundary Elements*, 27:101–105, 2003.

[3] A.I. Abreu, W.J. Mansur, and A. Canelas. Computation of time and space derivatives in a CQM-based BEM formulation. *Engineering Analysis with Boundary Elements*, 33:314–321, 2009.

[4] A.I. Abreu, W.J. Mansur, and J.A.M. Carrer. Initial conditions contribution in a BEM formulation based on the convolution quadrature method. *Int. J. Numer. Methods Eng.*, 67(3):417–434, 2006.

[5] A. Aimi, M. Diligenti, and C. Guardasoni. On the energetic Galerkin BEM applied to interior wave propagation problems. *J. Comput. Appl. Math.*, 235(7):1746–1754, 2011.

[6] S. Amini and S.M. Kirkup. Solution of helmholtz equation in the exterior domain by elementary boundary integral methods. *J. Comput. Phy.*, 118:208–221, 1995.

[7] D.N. Arnold and W.L. Wendland. On the asymptotic convergence of collocation methods. *Math. Comp.*, 41:197–242, 1983.

[8] D.N. Arnold and W.L. Wendland. The convergence of spline collocation for strongly elliptic equations on curves. *Numer. Math.*, 47:317–341, 1985.

[9] A. Bamberger and T. Ha Duong. Formulation variationelle pour le calcul de la diffraction d'une onde acoustique par une surface rigide. *Math. Meth. in the Appl. Sci.*, 8:598–608, 1986.

[10] L. Banjai and S. Sauter. Rapid solution of the wave equation in unbounded domains. *SIAM J. Numer. Anal.*, 47(1):227–249, 2008.

[11] D.J. Chappell. A convolution quadrature Galerkin boundary method for the exterior Neumann problem of the wave equation. *Math. Meth. Appl. Sci.*, 32:1585–1608, 2009.

[12] D. Colton. *Partial Differential Equations: An Introduction.* Random House, New York, 1988.

[13] M. Costabel. Time-dependent problems with the boundary integral equation method. In*: Encyclopedia of Computational Mechanics* (E. Stein, R. de Borst, T.J.R. Hughes, eds). John Wiley Sons, New York, 2004.

[14] V.J. Ervin, R. Kieser, and W.L. Wendland. Numerical approximation of the solution for a model 2-d hypersingular integral equation. *In: Coputational Engineering with Boundary Elements. Comput. Mech.*, 1:85–99, 1990.

[15] S. Falletta, G. Monegato, and L. Scuderi. Space-time boundary integral equation methods for non homogeneous wave equation problems. The Dirichlet case. *IMA J. Numer. Anal.*, 32(1):202–226, 2012.

[16] D. Givoli, T. Hagstrom, and I. Patlashenko. Finite element formulation with high-order absorbing boundary conditions for time-dependent waves. *Comput. Methods Appl. Mech. Engrg.*, 195:3666–3690, 2006.

[17] I.S. Gradshteyn and I.M. Ryzhik. *Table of Integrals, Series, and Products.* Academic Press, 2007.

[18] W. Hackbusch, W. Kress, and S. Sauter. Sparse convolution quadrature for time domain boundary integral formulations of the wave equation. *IMA J. Numer. Anal.*, 29:158–179, 2009.

[19] H. Kawaguchi and T. Weiland. Initial value problem formulation of time domain boundary element method for electromagnetic microwave simulations. *Eng. Anal. Boundary Elem.*, 36:968–978, 2012.

[20] L. Kielhorn and M. Schanz. Convolution quadrature method-based symmetric Galerkin boundary element method for 3-D elastodynamics. *Int. J. Numer. Methods Eng.*, 76:1724–1746, 2008.

[21] A.R. Laliena and F.-J. Sayas. Theoretical aspects of the application of convolution quadrature to scattering of acoustic waves. *Numer. Math.*, 112:637–678, 2009.

[22] I. Lasiecka and R. Triggiani. Sharp regularity theory for second order hyperbolic equations of Neumann type. I. L_2 nonhomogeneous data. *Ann. Mat. Pura Appl.*, 157(4):285–367, 1990.

[23] I. Lasiecka and R. Triggiani. Regularity theory of hyperbolic equations with nonhomogeneous Neumann boundary conditions. II. General boundary data. *J. Differential Equations*, 94(1):112–164, 1991.

[24] P.D. Lax and R.S. Phillips. *Scattering Theory*, volume 5. Academic Press, London, 1989.

[25] Ch. Lubich. Convolution quadrature and discretized operational calculus. I. *Numer. Math.*, 52:129–145, 1988.

[26] Ch. Lubich. On the multistep time discretization of linear initial-boundary value problems and their boundary integral equations. *Numer. Math.*, 67(3):365–389, 1994.

[27] Ch. Lubich. Convolution quadrature revised. *BIT*, 44:503–514, 2004.

[28] W.J. Mansur, D. Soares Jr., and M.A.C. Ferro. Initial conditions in frequency-domain analysis: the FEM applied to the scalar wave equation. *J. Sound and Vibration*, 270:767–780, 2004.

[29] P.A. Martin and F.J. Rizzo. On the boundary integral equations for crack problems. *Proc. R. Soc. Lond. A*, 421:341–355, 1989.

[30] G. Monegato. Numerical evaluation of hypersingular integrals. *J. Comput. Appl. Math.*, 50:9–31, 1994.

[31] G. Monegato. Definitions, properties and applications of finite part integrals. *J. Comput. Appl. Math.*, 229(2):425–439, 2009.

[32] G. Monegato and L. Scuderi. High order methods for weakly singular integral equations with non smooth input functions. *Math. Comp.*, 67:1493–1515, 1998.

[33] G. Monegato and L. Scuderi. Numerical integration of functions with boundary singularities. *J. Comput. Appl. Math.*, 112:201–214, 1999.

[34] G. Monegato and L. Scuderi. Potential evaluation in space-time BIE methods. *J. Comput. Appl. Math.*, 243:60–79, 2013.

[35] G. Monegato, L. Scuderi, and M.P. Stanić. Lubich convolution quadratures and their application to space-time BIEs. *Numerical Algorithms*, 56(3):405–436, 2011.

[36] C.S. Morawetz. Decay for solutions of the exterior problem for the wave equation. *Comm. Pure Appl. Math.*, 28:229–264, 1975.

[37] W. Moser, H. Antes, and G. Beer. Soil-structure interaction and wave propagation problems in 2D by a Duhamel integral based approach and the convolution quadrature method. *Comput. Mech.*, 36:431–443, 2005.

[38] J.C. Nédélec. Approximation of integral equations by finite elements. Ch. XIII. *In: Mathematical analysis and numerical methods for science and technology (R. Dautray, J.L. Lions, eds.)*, pages 359–370, Springer, 1990.

[39] A.P. Prudnikov, Yu.A. Brychkov, and O.I. Marichev. *Integrals and Series*, volume 5. New York: Gordon and Breach, 1992.

[40] M. Schanz, T. Rüberg, and L. Kielhorn. Time domain BEM: numerical aspects of collocation and Galerkin formulations. *In: Recent Advances in Boundary Element Methods (G.D. Manolis, D. Polyzos, eds.)*, pages 415–432, Springer Science, 2009.